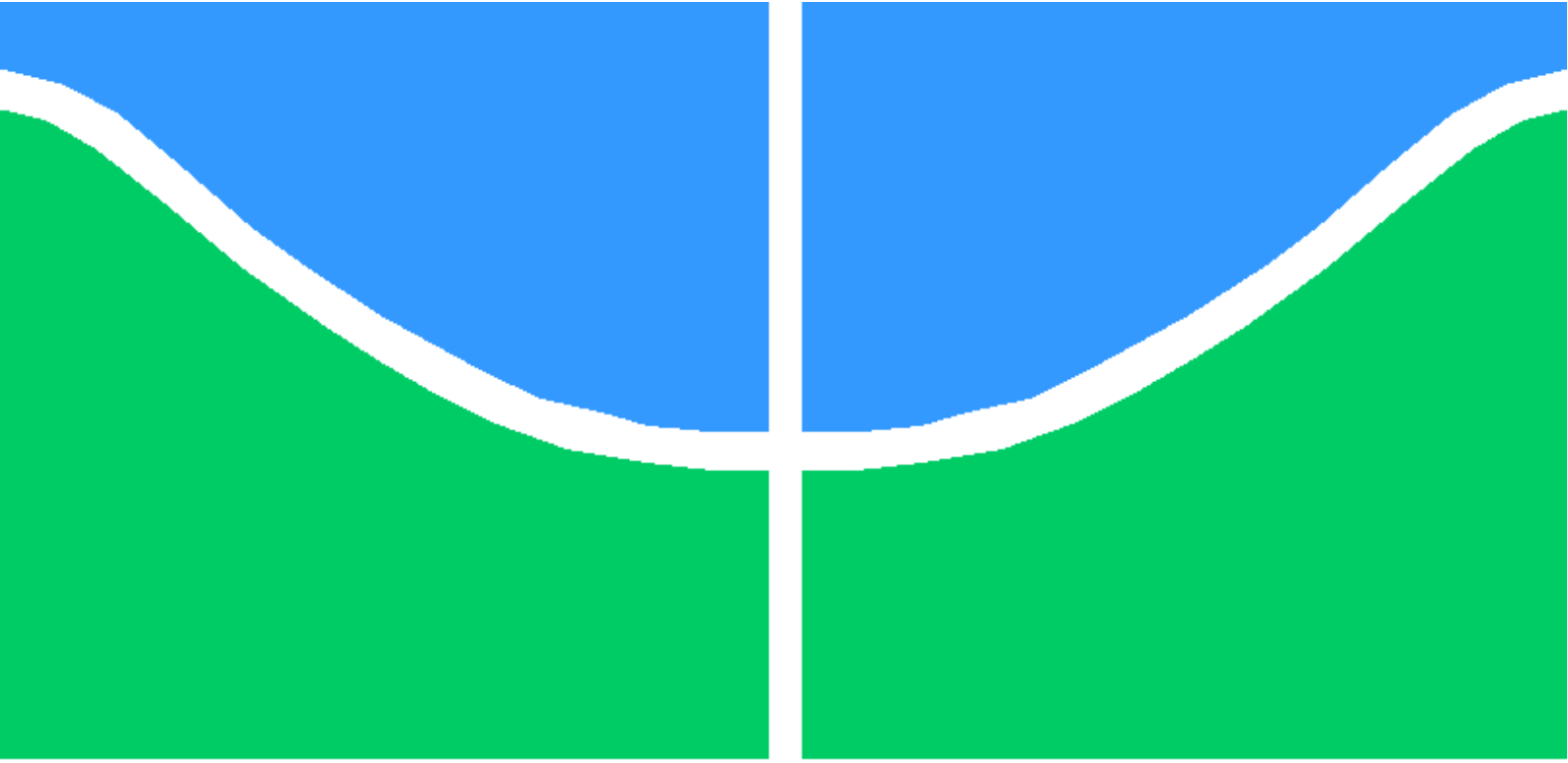

Universidade de Brasília - UnB
Faculdade de Tecnologia - FT
Engenharia Elétrica

Tensor-based Tracking Schemes for Time-Delay Estimation in GNSS Multi-antenna Receivers

Autor: Caio César Rodrigues Garcez
Orientador: Prof. Dr. João Paulo Carvalho Lustosa da Costa

Brasília, DF
07 de julho de 2017

Caio César Rodrigues Garcez

Tensor-based Tracking Schemes for Time-Delay Estimation in GNSS Multi-antenna Receivers

Monografia submetida ao curso de graduação em Engenharia Elétrica da Universidade de Brasília, como requisito parcial para obtenção do Título de Bacharel em Engenharia Elétrica.

Universidade de Brasília - UnB

Faculdade de Tecnologia - FT

Supervisor: Prof. Dr. João Paulo Carvalho Lustosa da Costa

Co-supervisor: Daniel Valle de Lima

Brasília, DF

07 de julho de 2017

Caio César Rodrigues Garcez

Tensor-based Tracking Schemes for Time-Delay Estimation in GNSS Multi-antenna Receivers/ Caio César Rodrigues Garcez. – Brasília, DF, 07 de julho de 2017-

87 p. : il. (algumas color.) ; 30 cm.

Supervisor: Prof. Dr. João Paulo Carvalho Lustosa da Costa

Trabalho de Conclusão de Curso – Universidade de Brasília - UnB
Faculdade de Tecnologia - FT , 07 de julho de 2017.

1. Array Signal Processing. 2. Global Navigation Satellite Systems. I. Prof. Dr. João Paulo Carvalho Lustosa da Costa. II. Universidade de Brasília. III. Faculdade de Tecnologia. IV. Tensor-based Tracking Schemes for Time-Delay Estimation in GNSS Multi-antenna Receivers

CDU 02:141:005.6

Caio César Rodrigues Garcez

Tensor-based Tracking Schemes for Time-Delay Estimation in GNSS Multi-antenna Receivers

Monografia submetida ao curso de graduação em Engenharia Elétrica da Universidade de Brasília, como requisito parcial para obtenção do Título de Bacharel em Engenharia Elétrica.

Trabalho aprovado. Brasília, DF, 07 de julho de 2017:

Prof. Dr. João Paulo Carvalho Lustosa da Costa
Orientador

Prof. Dr. Ricardo Zelenovsky
Membro 1

Ricardo Kehrle Miranda
Membro 2

Brasília, DF
07 de julho de 2017

Agradecimentos

Em primeiro lugar, gostaria de agradecer ao professor João Paulo C. Lustosa da Costa pelo seu apoio, orientação e paciência durante a conclusão deste trabalho. Agradeço também aos meus orientadores Daniel Valle de Lima e Ricardo Kehrle Miranda por me fornecerem os recursos necessários para a execução do trabalho bem como períodos para o esclarecimento de dúvidas.

Gostaria de deixar um agradecimento especial ao meu avô Carlos Rodrigues Alves.

Abstract

Although Global Navigation Satellite Systems (GNSS) receivers nowadays achieve high accuracy when processing their geographic location under conditions of Line of Sight (LOS), errors due to interference by multipath and noise are the most degrading sources of accuracy. In order to solve the multipath interference, receivers based on multiple antennas have become the focus of technological research and development due to the fact they can mitigate multipath occurrence providing best estimates to the transmitted signal time-delay, which is a relevant parameter for determining the user's geolocation. In this context, tensor-based approaches based on PArallel FActor Analysis (PARAFAC) models have been proposed in the literature, providing optimal performance. As these techniques are subspace-based, considering a real-time tracking scenario, the computation of a full Eigenvalue Decomposition (EVD)/Singular Value Decomposition (SVD) for signal subspace estimation at every sampling instant is not suitable, due to complexity reasons. Therefore, an alternative to reduce the Time of Computing (ToC) of subspace estimations has been the development of subspace tracking algorithms. This work proposes the employment of two subspace tracking schemes to provide a reduction in the overall computational performance of tensor-based time-delay estimation techniques.

Key-words: Navigation. Satellites. GNSS receiver. Uniform Linear Array. Direction of Arrival. Correlation. Tracking.

Resumo

Embora os receptores GNSS (Global Navigation Satellite Systems) alcancem atualmente alta precisão ao processar sua localização geográfica sob condições de Linha de Visão (Line of Sight), erros devido a interferência por componentes multipercurso e ruído são as fontes mais degradantes desse sistema. A fim de resolver a interferência multipercurso, receptores baseados em múltiplas antenas tornaram-se o foco de pesquisa e desenvolvimento tecnológico devido ao fato de que podem mitigar a ocorrência de multipercurso fornecendo as melhores estimativas para o atraso do sinal transmitido, que é um parâmetro relevante para determinar a geolocalização do usuário. Neste contexto, abordagens tensoriais baseadas em modelos PARAFAC (PArallel FActor Analysis) têm sido propostas na literatura, proporcionando um ótimo desempenho. Como essas técnicas são baseadas em subespaços, considerando um cenário de rastreamento em tempo real, o cálculo de uma EVD (Eigenvalue Decomposition)/SVD (Singular Value Decomposition) completa para estimativa de subespaço de sinal em cada instante de amostragem não é adequado, devido a razões de complexidade. Portanto, uma alternativa para reduzir o tempo de computação (Time of Computing) de estimativas de subespacos tem sido o desenvolvimento de algoritmos de rastreamento de subespaço. Este trabalho propõe o emprego de dois esquemas de rastreamento de subespaços para fornecer uma redução no desempenho computacional geral das técnicas de estimativa de atraso de tempo baseadas em tensores.

Palavras-chave: Navegação. Satélites. Receptores GNSS. Arranjo Linear Uniforme. Correlação. Rastreamento.

List of Figures

List of Tables

List of abbreviations and acronyms

GNSS	Global Navigation Satellite Systems.
LOS	Line of Sight.
MI	Multipath Interference.
NLOS	Non Line Of Sight.
SCA	Security Critical Applications.
LCA	Liability Critical Applications.
PARAFAC	Parallel Factor Analysis.
DoA/KRF	Direction of Arrival/Khatri-Rao Factorization.
EVD	Eigenvalue Decomposition.
SVD	Singular Value Decomposition.
ToC	Time of Computing.
RFI	Radio Frequency Interference.
GPS	Global Positioning System.
GLONASS	GLObal'naya NAvigasionnay Sputnikovaya Systema.
SV	Spacial Vehicle.
ToA	Time of Arrival.
SPS	Standard Positioning Service.
AS	Augmentaton System.
UHF	Ultra High Frequency.
RF	Radio frequency.
MA	Multiple Access.
DS-CDMA	Direct-Sequence Code Division Multiple Access.
DSSS	Direct Sequence Spread Spectrum.

C/A	Coarse Acquisition Code.
P(Y)	Precise Encrypted Code.
LFSR	Linear Feedback Shift Register.
(M)	Navigation Data.
BPSK	Binary Phase Shift Keying.
AWGN	Additive White Gaussian Noise.
ULA	Uniform Linear Array.
ESPRIT	Estimation of Signal Parameter via Rotational Invariance Technique.
KRF	Khatri-Rao Factorization.
FBA	Forward-Backward Averaging.
ESPS	Expanded Spatial Smoothing.
PAST	Projection Approximation Subspace Tracking.
PCA	Principal Component Analysis.
RLS	Recursive Least Squares.
FDPM	Fast Data Projection Method.
DPM	Data Projection Method.
MAC	Multiply Accumulate.
FLOP	FLoating point OPeration.
RMSE	Root Mean Squared Error.
OSRMSE	Orthonormality Subspace Root Mean Squared Error.

Contents

Aspects of the work

0.1 Motivation

Although Global Navigation Satellite Systems (GNSS) receivers nowadays achieve high accuracy when processing their geographic location under conditions of Line of Sight (LOS), errors due to interference by multipath and noise are the most degrading sources of accuracy in GNSS systems.

Multipath Interference (MI) occurs when the user's device receives Non Line Of Sight (NLOS) reflected signals in addition to the LOS signal. These interfering signals are usually reflected from the ground, buildings, and other objects near the receiver. The Figure (1) illustrates the scenario.

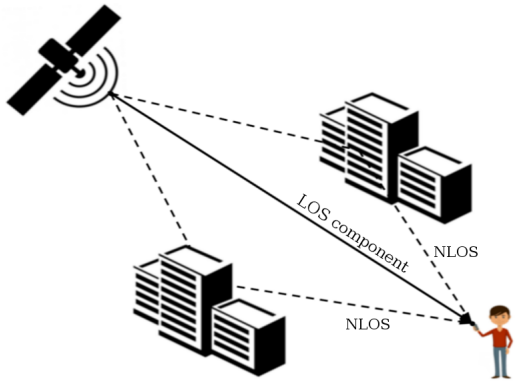

Figure 1 – Signal transmission with multipath occurrence.

0.2 Objective

In order to mitigate multipath components, several techniques using one single polarization antenna have been proposed in the literature, e. g. [4] [5], but their capabilities are not sufficient for safety-critical applications (SCA) or liability critical applications (LCA). Thus, multi-antenna systems became the focus of research and technological development. In this context, tensor-based approaches based on Parallel Factor Analysis (PARAFAC) models [2] have been developed, providing optimal performance. The current state-of-the-art tensor-based multipath mitigation technique applied to time-delay estimation is referred as the DoA/Khatri-Rao Factorization (DoA/KRF) [1]. As this technique is subspace-based, when considering its implementation in a real-time tracking scenario, the computation of a full EVD/SVD for signal subspace estimation at every sampling instant is not suitable, due to complexity reasons. Therefore, an alternative to reduce the

Time of Computing (ToC) of subspace estimations has been the development of subspace tracking algorithms. In this work we propose the employment of two subspace tracking schemes to provide a reduction in the overall computational performance of tensor-based time-delay estimation techniques.

0.3 Organization

The work is composed in three parts:

- Part [I]: Introduction.

  Chapter (1) introduces to basic concepts necessary for the understanding of GNSS systems. Chapter (2) deals with the characteristics of the transmitted signal for the Global Positioning System (GPS) technology related to its second generation.

- Part [II]: Data model.

  Chapter (3) derives the data model for the signal reception. The multi-antenna configuration is presented along with state-of-the-art signal processing techniques for time delay estimation. Chapter (4) presents the tracking scenario along with the derivation of the proposed tensor-based tracking techniques.

- Part [III]: Simulations and results.

  Chapter (5) presents the simulated results for the serial data sliding window tracking scenario.

0.4 Notation

In order to simplify the distinction between scalars, vectors, matrices and higher order tensors, this work adopts the following notation:

Scalars are denoted by lower-case letters:

$$\{a, b, c, \ldots, \alpha, \beta, \ldots\} \in \mathbb{C}^{1\times 1}$$

R-dimensional vectors are written as bold lower case letters:

$$\{\mathbf{a}, \mathbf{b}, \mathbf{c}, \ldots, \boldsymbol{\alpha}, \boldsymbol{\beta}, \ldots\} \in \mathbb{C}^{R\times 1}$$

$I \times J$ matrices correspond to bold-face capitals:

$$\{\mathbf{A}, \mathbf{B}, \ldots, \boldsymbol{\Sigma}, \boldsymbol{\Gamma}, \ldots\} \in \mathbb{C}^{I\times J}$$

The entry with row index i and column index j in a matrix $\mathbf{A}$, i.e. , $\mathbf{A}_{ij}$, is symbolized by a_{ij}.

For a given $Q < N$, given a matrix $\mathbf{A} \in \mathbb{C}^{M \times N}$, such that:

$$\mathbf{A} = \begin{bmatrix} \mathbf{a}_1 & \cdots & \mathbf{a}_{\mathrm{Q}} & \cdots & \mathbf{a}_n & \cdots & \mathbf{a}_N \end{bmatrix} \in \mathbb{C}^{M \times N}$$

The selection of the first Q columns of $\mathbf{A}$ is denoted as:

$$[\mathbf{A}]_{\uparrow_Q} = \begin{bmatrix} \mathbf{a}_1 & \cdots & \mathbf{a}_{\mathrm{Q}} \end{bmatrix} \in \mathbb{C}^{M \times Q}$$

The suppression of the first Q columns of $\mathbf{A}$ is denoted as:

$$[\mathbf{A}]_{\downarrow_Q} = \begin{bmatrix} \mathbf{a}_{\mathrm{Q}+1} & \cdots & \mathbf{a}_N \end{bmatrix} \in \mathbb{C}^{M \times N-Q}$$

To select a column of index n in the matrix $\mathbf{A} \in \mathbb{C}^{M \times N}$, the following notation is adopted:

$$\mathbf{A}_{(:,\mathrm{n})} = \mathbf{a}_n \in \mathbb{C}^{M \times 1}$$

Now considering each row of the matrix $\mathbf{A} \in \mathbb{C}^{M \times N}$, the selection of the first Q rows is denoted as:

$$[\mathbf{A}]_{\rightarrow_Q} \in \mathbb{C}^{Q \times N}$$

Higher order tensors are written as calligraphic letters:

$$\{\boldsymbol{\mathcal{A}}, \boldsymbol{\mathcal{B}}, \ldots\} \in \mathbb{C}^{I \times J \times K \times \ldots}$$

Information on the notation of operators is exposed in the Appendix (5.3).

Part I

Introduction

1 Concepts of Global Navigation Satellite Systems

1.1 Introduction

Satellite-based navigation systems establish geospatial positioning through the use of artificial satellites. These systems allow receivers on the Earth's surface to determine their geolocation by means of the transmitted signals, acquiring their position in a convenient spatial reference system. The accuracy of the location will be given according to the type of positioning technique used. When a satellite navigation system has the capability to provide positioning at any point on the earth's surface, the Global Navigation Satellite System (GNSS) nomenclature is adopted [6].

The current scenario consists of the modernization and improvement of the first GNSS systems: the United States GPS (Global Positioning System) and the Russian GLONASS (GLObal'naya NAvigasionnay Sputnikovaya Systema). In addition, new systems are in employment phase, these being important to emphasize the European GALILEO and the Chinese BeiDou.

In line with so many augmentation systems and activities in progress: satellite launching, new component technologies and the emergence of new signals and systems models, it becomes difficult to keep up with the latest developments. This rapid pace of progress expresses the continuous search for technologies that effectively promote a significant improvement in the accuracy and integrity of GNSS systems.

1.2 Components

GNSS systems are composed of three segments: the space segment, the control segment and the user segment. The space segment consists of the orbiting Spacial Vehicle (SV) that provides signals containing navigation data to the user's receiver. The control segment are reference stations scattered around the globe to monitor, correct and track satellites in space. Finally, the user segment composed of the receivers that perform the determination of the user's position from the signals transmitted by the satellites in order to provide navigation, synchronization, among other requisitions. These segments are almost similar in all satellite technologies currently found. Figure (2) illustrates each segments.

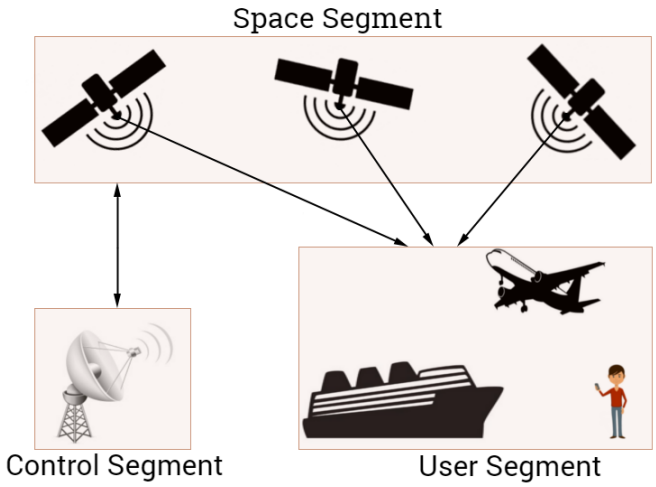

Figure 2 – GNSS segments.

1.3 Applications

The application of GNSS systems is a category with a wide range of areas such as location-based services, civil navigation, surveying and geographical mapping, maritime navigation research, agriculture, autonomy, science, space, road flow, military operations, among others. In addition, it is worth mentioning other recent applications of GNSS systems such as automatic toll vehicles [7], stand-alone vehicles that require high standards of safety and precision [8], real-time fishing ships location in order to guarantee the sustainable management of the fishing commonwealth [9] and precision farming, where the GNSS system is used to improve, for example, precise application of fertilization and also to coordinate handling 24 hours a day of expensive agricultural machines [10].

1.4 Fundamentals

Satellite-based navigation systems determine the user's position according to pseudorange measurements between the receiver and a set of visible satellites. These distances are calculated thought the Time of Arrival (ToA) which is the interval the transmitted signal takes to travel from the satellite to the receiver. This time corresponds to an observed carrier-phase difference among the satellite broadcasted signal and the received one.

Throughout the convention of expressing the user's position based on a three-dimensional coordinate system: $\{x, y, z\} = \mathbb{R}^3$ and a clock bias variable Δb related to the synchronization of the clock of the satellite system and the receiver's, a non-linear Euclidian system [6] can be solved for the four variables in order to obtain unambiguously the user's position. Since the satellites' position are known, it becomes necessary, regardless of the adopted GNSS system, that the orbits of the satellites must be chosen such that

for any place in the globe, the receiver will be available to visualize at least 4 satellites. The Figure (3) illustrates the positioning scenario.

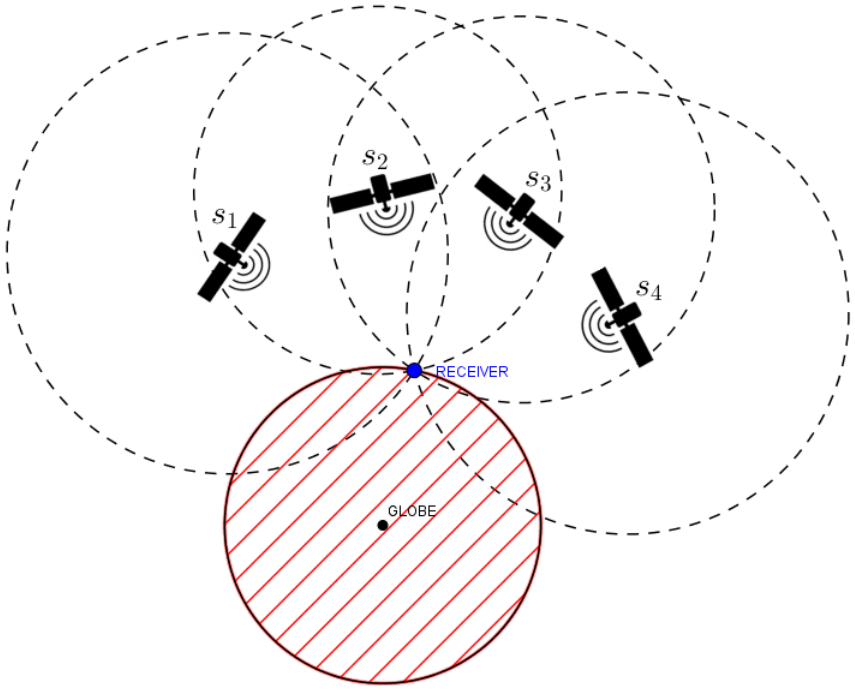

Figure 3 – Positioning process for a general receiver.

1.4.1 The Global Positioning System - GPS

The Global Positioning System (GPS) became the first operational GNSS system. It is operated by the United States and presently provides two services: one for civilian users, referred to as the Standard Positioning Service (SPS), and one restricted to military forces. In this work, the GPS system will be adopted as reference for the study of GNSS systems.

Generation	Number of satellites	Status
Block II-A	0	Nonoperational.
Block II-R	12	Operational.
Block IIR-M	7	Operational.
Block II-F	12	Operational.
GPS III	0	In production.

Table 1 – GPS constellation status.

Until the present moment of this work, the GPS constellation involves a mix of old and new satellites. The operational SVs are part of the Block II series which stands for the second generation of satellites: The Block II-A (Advanced), Block II-R (Replenishment), Block IIR-M (Modernized) and Block II-F (Follow-on). It is also important to mention

the forthcoming GPS III which is the next generation of SVs. The Table (1) points out a total of 31 operational satellites in the GPS constellation and their status.

1.4.2 GLONASS

Similar to the GPS system, the Russian system GLONASS uses 24 satellites. Originally, the intention was strictly militaristic. However, in 2007, Russia made GLONASS available for civilian and commercial use. Most of the actual receivers have an architecture compatible to GLONASS.

While GPS is the more accurate in most areas of the world, the Russian GLONASS system seems to operate more efficiently at northern latitudes as the purpose of GLONASS was to operate in Russia, home of the highest latitudes on the planet.

1.4.3 GALILEO

Galileo is an European system developed with the intend to offer basic navigation solution free of charge. The positioning services are more accurate when compared to any other system. Once full operational, Galileo will be available to users worldwide though the European Union.

1.4.4 BeiDou

China's Beidou satellite navigation system operates with 27 satellites that service the Asia-Pacific region, but current plans include global expansion to 30 satellites by 2020. The current system is accurate to within five meters and has designs on improvements to reach accuracy measurements within centimeters in order to compete with other solutions.

1.4.5 Augmentaton sytems

An Augmentaton System (AS) refers to any solution that helps improving the exactness, reliability, availability, or various other aspects of a GNSS receiver device. Several Augmentaton Systems have been developed for both military and civilian users. In order to meet the needs of both sectors, the US government has developed several types of augmentation systems, which have been made available to the public. Some of these systems include: ground-based systems, reference stations and support systems.

2 GNSS Signal and System Model

2.1 The GPS Signal

In order to describe the GPS signal model referred to the present moment of this work, the GPS 200 Interface Specification (IS-GPS-200) [11] will be adopted as reference. The IS-GPS-200 defines the characteristics of a signal transmitted from the operational Block II satellite series.

The GNSS signals are transmitted on the radio spectrum about 1.2 and 1.6 GHz in the Ultra High Frequency (UHF) band at a part of the L-band. This frequency range has been chosen for these signals since it enables measurements of adequate precision for a given simple user equipment and less signal attenuation from the atmosphere, under common weather conditions.

The GPS signals are broadcasted on two radio carriers denoted as L1 and L2. They are derived from a common frequency, $f_0 = 10.23$ MHz such that $f_{L1} = 154 f_0 = 1575.42$ MHz and $f_{L2} = 120 f_0 = 1227.60$ MHz. The Table (2) shows the signal content of each carrier component [12].

	L1 Link		**L2 Link**	
SV	**In phase**	**Quadrature**	**In phase**	**Quadrature**
Block II	P(Y) $\otimes$ D(t)	C/A(t) $\otimes$ D(t)	P(Y)	-
Block II-A	P(Y) $\otimes$ D(t)	C/A(t) $\otimes$ D(t)	P(Y)	-
Block II-R	P(Y) $\otimes$ D(t)	C/A(t) $\otimes$ D(t)	P(Y) $\otimes$ D(t)	-
Block IIR-M	P(Y) $\otimes$ D(t)	C/A(t) $\otimes$ D(t)	P(Y) $\otimes$ D(t)	L2 CM $\otimes$ D(t)
Block IIR-F	P(Y) $\otimes$ D(t)	C/A(t) $\otimes$ D(t)	P(Y) $\otimes$ D(t)	L2 CM $\otimes$ D(t)
GPS-III	P(Y) $\otimes$ D(t)	C/A(t) $\otimes$ D(t)	P(Y) $\otimes$ D(t)	L2 CM $\otimes$ D(t)

Table 2 – RF links components for the operational Block II series satellites.

As seen in Table (2) the GPS system carrier signal content may differ when considering in-phase and quadrature components for the L2 link. Thus, as this work has an approach for a civilian receiver, only the L1 RF link will be adopted.

Since several satellites need to share the same available channel bandwidth for the signal transmission, Multiple Access (MA) techniques are employed in order to ensure that signals from different satellites will be separated or even orthogonal to each other. This way the user is capable of identifying the transmitting satellites.

The GPS system protocol for MA is defined as Direct-Sequence Code Division Multiple Access (DS-CDMA), a form of CDMA. Each satellite has two unique Direct Sequence Spread Spectrum (DSSS). The first is know as the Coarse Acquisition Code

(C/A code), intended for civil applications. The other one is denoted as the Precise Encrypted Code (P(Y)), reserved to military forces. This work restricts to the use of the C/A code for the signal processing.

2.1.1 The C/A code

The C/A code consists of a sequence of 1023 chips. The bit is called a chip to emphasize that it does not carry information. The code repeats over a period of 1 ms with a baud rate of 10.23 MHz. We define the chip sequence by:

$$\mathbf{c} = \begin{bmatrix} c_1 & c_2 & \cdots & c_{1023} \end{bmatrix} \in \mathbb{N}^{1\times 1023} \tag{2.1}$$

2.1.2 Code Generation

The GPS C/A code is formed with two Linear Feedback Shift Registers (LFSR) of 10 registers driven with a clock frequency of 1.023 MHz. The tap positions of both registers are fixed, and their seeds are all one for all sequences. The code is created by adding specific taps of the first LFSR with other taps of the second LFSR. Different sequences are generated when tap positions of the LFSRs are modified.

The Figures (4) and (5) illustrate the LFSRs used for the generation of the C/A code for PRN=1. The register presented in the Figure (4) is detonated as G1. The other register illustrated on the Figure (5) is referred as G2. In order to illustrate the generation of other C/A code sequences, the Table (3) presents the convention for the tap positions of RG1 used for generating other four sequences. The entire convention can be viewed in [11].

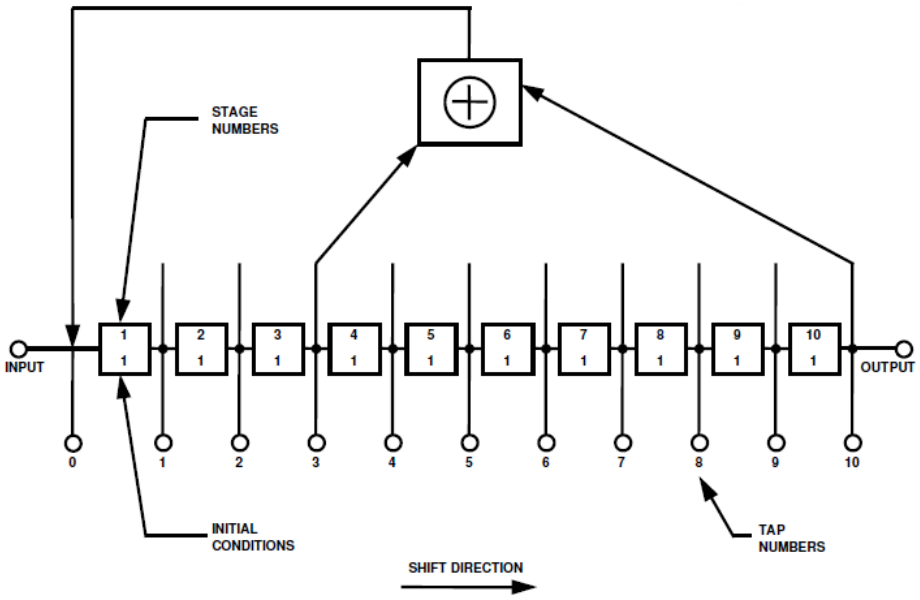

Figure 4 – G1 Shift Register Generator Configuration for PRN=1.

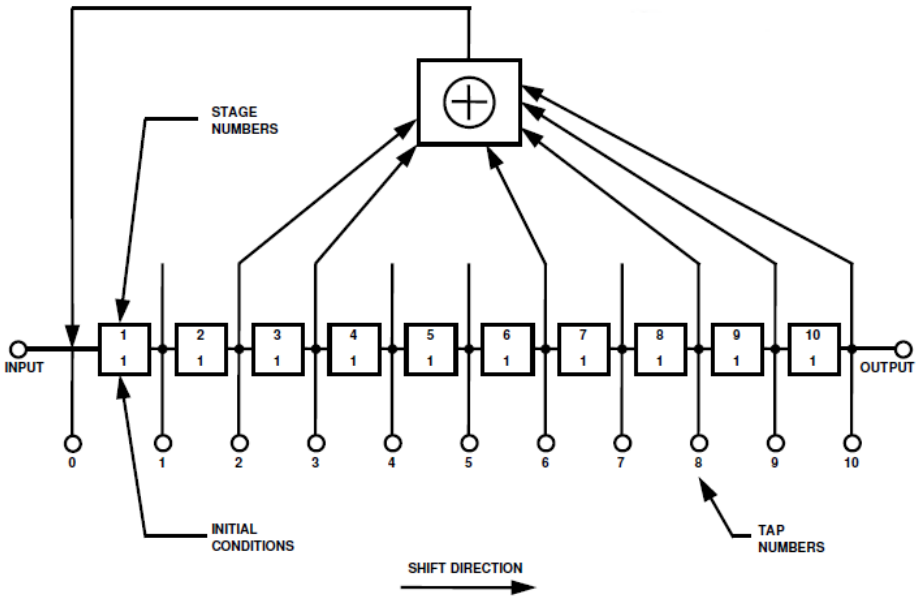

Figure 5 – G2 Shift Register Generator Configuration for PRN=1.

Sat ID	Tap selections
1	$2 \otimes 6$
2	$3 \otimes 7$
3	$4 \otimes 8$
4	$5 \otimes 9$
5	$1 \otimes 9$

Table 3 – Selection of different register taps in order to generate the first 5 C/A codes.

Considering the tap positions of the register G1, the polynomial p_{G1} of the register is given by: $p_{G1}(x) = x^{10} + x^3$. For the register G2: $p_{G2}(x) = x^{10} + x^9 + x^8 + x^6 + x^3 + x^2$. The C/A code bit is given by the modulo-2 sum of $p_{G1}(x)$ and $p_{G2}(x)$:

$$C/A(x) = (p_{G1}(x) \oplus p_{G2}(x)) \tag{2.2}$$

Which results in a code of length of 1023 chips. These codes are also refereed as Gold codes after the name of their inventor. One propriety is that they have low correlation for different code sequences. This indicates that if the C/A code of a satellite is correlated with either itself or with another, the result will be zero or close to zero, as indicated below:

$$\mathrm{E}\{\mathbf{c}_i[n] - \mathbf{c}_i[n-\tau]\} \approx 0\,, \quad \text{if } \tau \neq 0 \tag{2.3}$$

$$\mathrm{E}\{\mathbf{c}_i[n] - \mathbf{c}_j[n-\tau]\} \approx 0\,, \quad \text{if } i \neq j \tag{2.4}$$

Where E{ } denotes the expected value operator.

2.2 Navigation Data

Referred as (M), the Navigation Data is a binary-coded message consisting of three major components. The first part contains the GPS date and time plus the satellite's status and an indication of its health. The second part contains orbital information data, called ephemeris. It allows the receiver to calculate the position of the satellite. The third part, called the almanac, contains information concerning the status, location and C/A code number of all the satellites of the constellation. The navigation message is transmitted at 50 bits per second within a period of 20 ms. The Figure (6) shows the power density spectrum of the GPS signal containing the C/A code sequence along with the P(Y) code and the NAV(M) data.

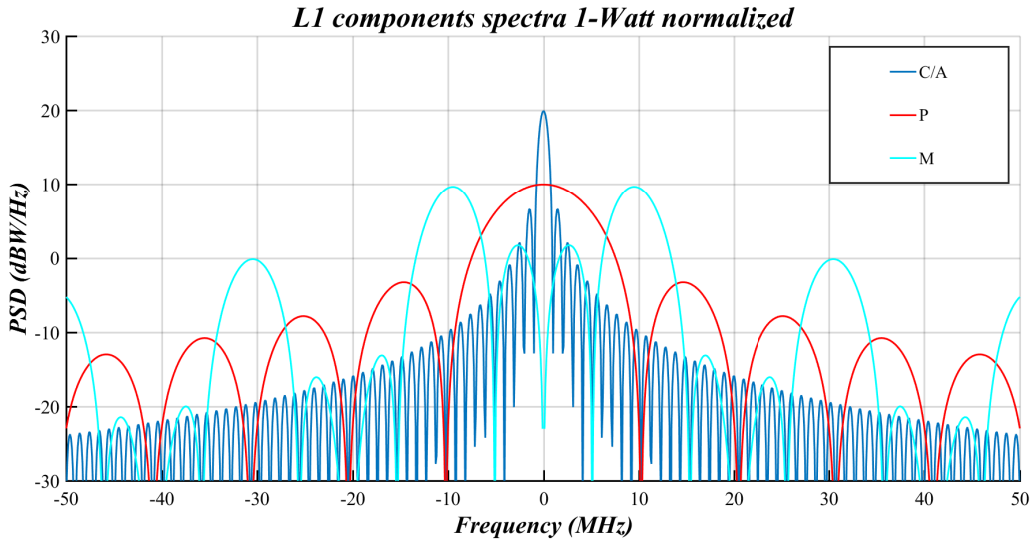

Figure 6 – C/A along with P(Y) code and NAV(M) data power density spectrum for PRN=1.

2.3 Modulation

2.3.1 Binary Phase Shift Keying

The Binary Phase Shift Keying (BPSK) is the modulation process most used for GNSS systems nowadays. In this method, a 0 bit does not change the transmitted carrier and a 1 bit multiplies the carrier by -1, which is equivalent to shift the phase of the sinusoidal signal by 180°.

2.3.2 BPSK-DSSS modulation

Direct Sequence Spread Spectrum (DSSS) technique adds the C/A code to the navigation data obtaining a higher symbol rate signal. The Figure (7) illustrates the modulation process. At the receiver, the demodulation process obtains the original navigation data by multiplying the incoming signal by the same C/A code sequence used in the modulation process.

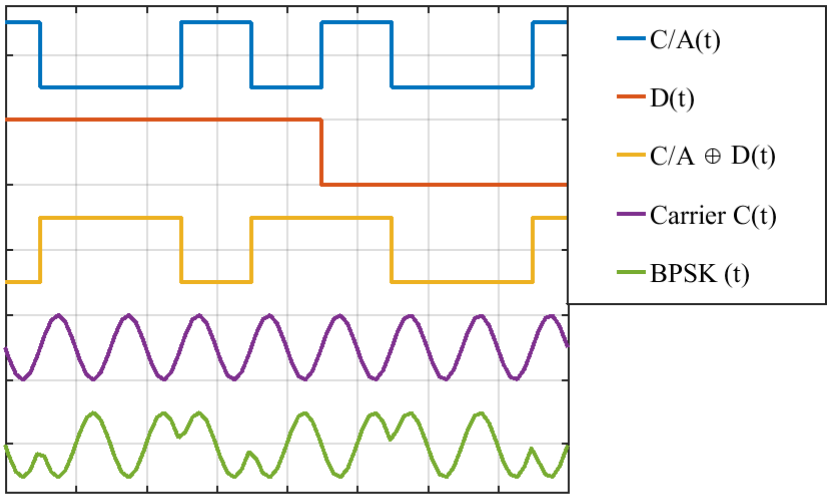

Figure 7 – BPSK-DSSS modulation of the C/A code along with the NAV data.

2.4 Transmitted signal model

As seen in Table (2), the L1 link consists of two carrier components which are in phase quadrature with each other. Each carrier component is BPSK-DSSS modulated by different bit trains. One bit train is the modulo-2 sum of the P(Y) code and NAV data, while the other is the modulo-2 sum of the C/A-code and the NAV data. Even though both codes are broadcast on L1, they are distinguishable from one another by their transmission in quadrature. That means that the C/A code modulation on the L1 carrier is phase shifted 90° from the P(Y) code modulation on the same carrier. Therefore, a model for the signal transmitted from the k-th satellite can be derived as [12]:

$$s^{(k)}(t) = \sqrt{2P_{P,L1}}(P^{(k)}(t) \oplus D^{(k)}(t))\cos(2\pi f_c t) + \sqrt{2P_{C/A,L1}}(C/A^{(k)}(t) \oplus D^{(k)}(t))\sin(2\pi f_c t) \tag{2.5}$$

Where $P_{P,L1}$ is the power of the signal with the P(Y) code, $P_{C/A,L1}$ is the power of the signal with the C/A code, $D(t)$ is the navigation data, $P(t)$ is the P(Y) code, $C/A(t)$ is the C/A code and f_c is the central frequency of the carrier.

Since the P(Y) code is restricted to military forces, only the quadrature component in Equation (2.5) will be considered in this work. Thus, The model for the transmitted signal becomes:

$$s^{(k)}(t) = \sqrt{2P_{C/A,L1}}(C/A^{(k)}(t)) \sin(2\pi f_c t) \tag{2.6}$$

Part II

Data model

3 Received Signal Model

3.1 Introduction

Most of the modern approaches to signal processing are model-based, in the sense that they rely on certain assumptions on the data observed in the real world. The received signal consists of a carrier denoted by:

$$s_\ell(t) = \alpha_\ell(t)\cos(2\pi f_c t + \beta_\ell(t)) \tag{3.1}$$

Where $\alpha(t)$ is the in-phase component, $\beta(t)$ the quadrature component. The index $\ell = [1, 2, \cdots, L]$ denotes the LOS component, referred as $(\ell = 1)$, and the remain $(L-1)$ NLOS copies.

Another expression can be obtained for Equation (3.1) by defining the cosine as a real part of a complex exponential, such that:

$$s_\ell(t) = \alpha_\ell(t)\,\Re\{e^{j2\pi f_c t + \beta_\ell(t)}\} \tag{3.2}$$

From Equation (3.2) it is possible to obtain the phasor expression for the received signal, denoted as $\bar{s}_\ell(t)$ which is defined as:

$$\bar{s}_\ell(t) = \alpha_\ell(t)e^{j2\pi f_c t + \beta_\ell(t)} \tag{3.3}$$

The nature of the signal in a complex domain form found in Equation (3.3) is supported by most GNSS receivers, which decompose the signal into both in-phase and quadrature components as seen in the section (2.4), such that only the quadrature component consisted of the C/A ranging code is of interest.

Throughout the description of the algorithms and derivation of the techniques, the following scenario is assumed [13]:

- **Isotropic and linear transmission medium**.

  The transmission medium between the satellites and the receiver is assumed to be isotropic and linear. In other words, the medium has the same physical properties in all different directions and the signals at any particular point can be superposed linearly. This means that, particularly for this work, the L received signals can be expressed as a linear superposition of the LOS component along with the $L-1$ NLOS components. In addition, it is important to mention that:

  – The propagation property of the signal waves do not change in relation to the direction of arrival of the signals.

– The gain of each antenna or sensor element is assumed to be unitary.

- **Far-field assumption**.

  The satellites are located far from the receiver such that the wavefront generated by each transmitted signal arrives at all the elements of the antenna array at an equal direction of propagation, leading to a planar impinging wavefront. The Figure (8) illustrates the scenario.

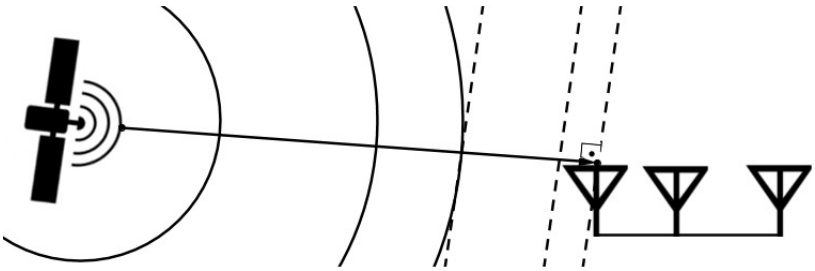

Figure 8 – Far-field transmission.

- **Narrowband assumption.** As the LOS component and the NLOS copies have the same carrier frequency, their frequency contents must be concentrated in the neighborhood of the carrier frequency f_c. In orther words, the therms $\alpha(t)$ and $\beta(t)$ in the equation (3.1) must vary slowly when the signal propagates from one antenna element to another on the multi-antenna receiver, see Figure (10).

- **AWGN Channel.** The noise is assumed to be of a complex white Gaussian process. The additive noise is taken from a zero mean, spatially uncorrelated random process, which is uncorrelated with the signals. The noises have a common variance σ_n^2 at all the array elements and are uncorrelated among all elements or sensors.

3.2 The Uniform Linear Array - ULA

The proposed multi-antenna receiver is configured as an Uniform Linear Array (ULA). This antenna array consists of M identical and omni-directional antenna elements aligned and equally spaced. The distance between the two adjacent elements is Δ. The ULA geometry is illustrated in the Figure (9).

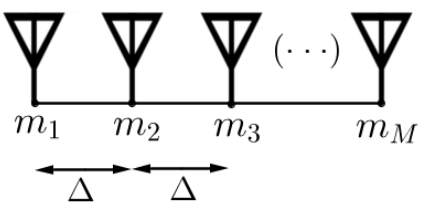

Figure 9 – Uniform Linear Array with M antennas.

The data model states that the LOS component transmitted by the k-th satellite impinges on the ULA-based antenna receiver at an angle θ_l. Therefore, the signal received by the first antenna is a delayed version of the transmitted signal expressed in equation (3.1) with a delay of τ_d which is the time the signal takes to travel from the satellite to reach the first antenna element of the receiver. That is:

$$\bar{s}_{\ell,1}(t) = \bar{s}_{\ell}(t-\tau_d) = \alpha_{\ell}(t-\tau_d)e^{j2\pi f_c(t-\tau_d)+\beta_{\ell}(t-\tau_d)} \tag{3.4}$$

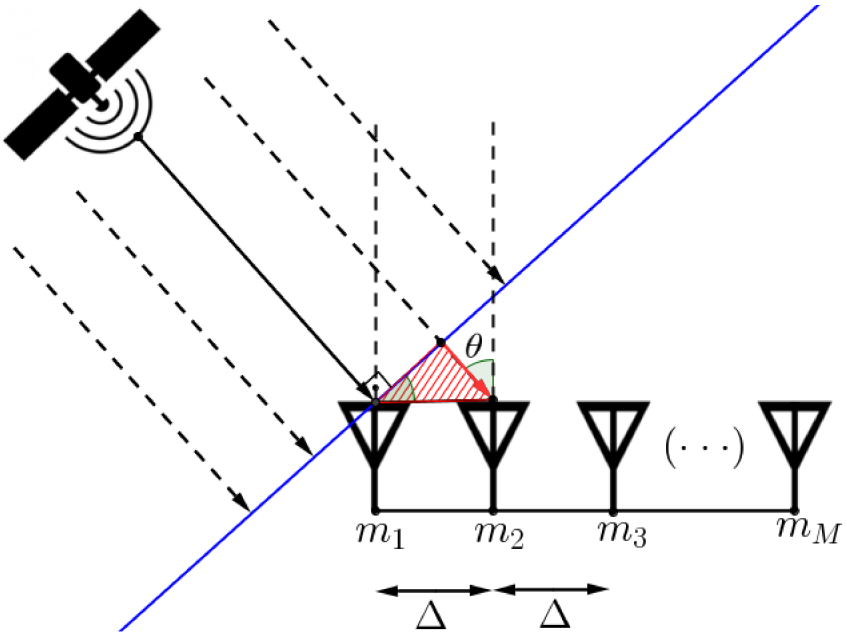

Figure 10 – The scenario under consideration.

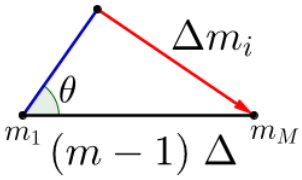

Figure 11 – Triangle formed between the first and m-th antenna.

The ULA places each element equally spaced such that is possible to form the triangle in the Figure (11) for the remaining antennas. The only difference relies on the element position which will increase the distance by $(m-1)$. Thus, the general expression for the m-th element is:

$$\Delta m_i = (m-1)\Delta \sin(\theta_{\ell}) \tag{3.5}$$

Where $m = [1, 2, \cdots, M]$. The received signal of the m-th element is a delayed version of $s_{\ell,1}(t)$. This additional delay is given by:

$$\tau_{mi} = \frac{\Delta m_i}{c} \tag{3.6}$$

From the Equations (3.5) and (3.6) we can write:

$$\tau_{mi} = (m-1)\frac{\Delta \sin(\theta_\ell)}{c} \tag{3.7}$$

Thus, from Equations (3.4) and (3.7) we can write the expression for the received signal by the m-th element as:

$$\bar{s}_{\ell,m}(t) = \bar{s}_{\ell,1}(t-\tau_{mi}) = \bar{s}_\ell(t-\tau_d-\tau_{mi}) \tag{3.8}$$

$$\bar{s}_{\ell,m}(t) = \alpha_\ell(t-\tau_d-\tau_{mi})e^{j2\pi f_c(t-\tau_d-\tau_{mi})+\beta_\ell(t-\tau_d-\tau_{mi})} \tag{3.9}$$

Accordion to the narrowband assumption, the in-phase and quadrature components will not change during the propagation between each antenna element, such that the Equation (3.9) becomes:

$$\bar{s}_{\ell,m}(t) = \alpha_\ell(t-\tau_d)e^{j2\pi f_c(t-\tau_d-\tau_{mi})+\beta_\ell(t-\tau_d)} \tag{3.10}$$

$$\bar{s}_{\ell,m}(t) = \alpha_\ell(t-\tau_d)e^{j2\pi f_c(t-\tau_d)+\beta_\ell(t-\tau_d)}e^{-j2\pi f_c\tau_{mi}} \tag{3.11}$$

$$\bar{s}_{\ell,m}(t) = \bar{s}_{\ell,1}(t)e^{-j2\pi f_c\tau_{mi}} \tag{3.12}$$

From the Equation (3.7) we replace an expression for τ_{mi} in the Equation (3.12), such that:

$$\bar{s}_{\ell,m}(t) = \bar{s}_{\ell,1}(t)e^{-j2\pi f_c(m-1)\frac{\Delta \sin(\theta_\ell)}{c}} \tag{3.13}$$

Defining $\mu_\ell = -\frac{2\pi f_c}{c}\Delta \sin(\theta_\ell)$ as the spatial frequency associated with the l-th signal component and replacing $c = \lambda f_c$ obtaining $\mu_\ell = -\frac{2\pi}{\lambda}\Delta \sin(\theta_\ell)$, the Equation (3.13) can be rewritten as:

$$\bar{s}_{\ell,m}(t) = \bar{s}_{\ell,1}(t)e^{j(m-1)\mu_\ell} \tag{3.14}$$

Equation (3.14) shows that the signal received by the m-th element from the l-th signal component is the same as that received by the first (leftmost) element but with an additional phase shift factor of $e^{j(m-1)\mu_\ell}$. This factor depends only on the spatial frequency μ_ℓ, and the position of the m-th element relative to the first element.

As the spacial frequency depends on θ_ℓ. For each incident θ_ℓ related to a signal component, there is a corresponding spatial frequency μ_ℓ. The objective of the Direction of Arrival (DoA) estimation is to obtain the spatial frequencies from the L signals received by the array. A DoA scheme with good accuracy and low computational complexity is presented in [14] as the Estimation of Signal Parameter via Rotational Invariance Technique (ESPRIT) which requires a shift invariant array response. The ESPRIT algorithm is detailed in Subsection (3.5.1).

Now considering the Isotropic and linear transmission medium, all the L incident signals components can be superposed such that the overall signal $x(t)$ received by the m-th element of the array can be expressed as:

$$x(t) = \sum_{\ell=1}^{L} \sum_{m=1}^{M} \bar{s}_{\ell,1}(t) e^{j(m-1)\mu_\ell} \tag{3.15}$$

For the sake of simplicity, the signal $\bar{s}_{\ell,1}(t)$ received by the fist antenna element will be denoted as $s_\ell(t)$. Considering the AWGN characteristics of the channel, the signal $x(t)$ can be written as:

$$x(t) = \sum_{\ell=1}^{L} \sum_{m=1}^{M} s_\ell(t) e^{j(m-1)\mu_\ell} + n(t) \tag{3.16}$$

A convenient way to analyze Equation (3.16) is to express the signal in the matrix form. That is considering:

$$\mathbf{a}(\theta_\ell) = \begin{bmatrix} 1 & e^{j\mu_\ell} & \cdots & e^{j(m-1)\mu_\ell} \end{bmatrix}^{\mathrm{T}} \in \mathbb{C}^{M\times 1} \tag{3.17}$$

Where $\mathbf{a}(\theta_\ell)$ in Equation (3.17) is referred as the steering vector which contains the additional phase shift factor for each antenna element in the array.

By concatenating the l steering vectors, we define the steering matrix $\mathbf{A}(\boldsymbol{\theta})$ in the following fashion:

$$\mathbf{A}(\boldsymbol{\theta}) = \begin{bmatrix} \mathbf{a}(\theta_1) & \mathbf{a}(\theta_2) & \cdots & \mathbf{a}(\theta_\ell) \end{bmatrix}^{\mathrm{T}} \in \mathbb{C}^{M\times L} \tag{3.18}$$

Considering $s(t)$ as a discrete time signal $s[n]$ such that $n = [1, 2, \cdots, N]$ are the number of samples, the signal vector $\mathbf{s}_\ell$ is given by:

$$\mathbf{s}_\ell = \begin{bmatrix} s_\ell[1] & \cdots & s_\ell[n] \end{bmatrix} \in \mathbb{C}^{1\times N} \tag{3.19}$$

Concatenating the l signal vectors, we define the signal matrix $\mathbf{S}$ below:

$$\mathbf{S} = \begin{bmatrix} \mathbf{s}_1[n] & \cdots & \mathbf{s}_\ell[n] \end{bmatrix}^{\mathrm{T}} \in \mathbb{C}^{L\times N} \tag{3.20}$$

Therefore, the received signal $\mathbf{x}[n]$ can be expressed in a matrix fashion by:

$$\mathbf{X} = \mathbf{AS} + \mathbf{N} \tag{3.21}$$

Equation (3.21) establishes the signal model to be adopted in this work. In the next sections this data model will be used throughout the derivation of the pre and post-correlation signal models for the GNSS ULA-based receiver.

3.3 Pre-correlation signal model

Based on the signal model for an ULA receiver derived in Section (3.2) through the Equation (3.16) and its matrix form expressed in Equation (3.21), the L received signals for the ULA-based GNSS receiver [15] can be expressed as a linear superposition of the LOS component along with the $L-1$ NLOS replicas. Such that:

$$\mathbf{x}(t) = \sum_{\ell=1}^{L} \mathbf{s}_\ell(t) + n_\ell(t) \tag{3.22}$$

Where $\mathbf{s}_\ell(t)$ can be expressed as:

$$\mathbf{s}_\ell(t) = \mathbf{a}(\phi_\ell)\, \gamma_\ell\, \mathbf{c}^{\mathrm{T}}[t-\tau_\ell] \tag{3.23}$$

Where $\mathbf{a}(\phi_\ell) \in \mathbb{C}^{\mathrm{M}\times 1}$ is referred as the steering vector with azimuth angle of ϕ_ℓ. The vector $\mathbf{c}[t-\tau_\ell] \in \mathbb{C}^{1\times N}$ denotes the C/A code sequence with time delay τ_ℓ and γ_ℓ is a complex amplitude. The additive complex white Gaussian noise is referred as $n_\ell(t)$.

Since each C/A code contains $N = 1023$ samples and can be temporally grouped into K epochs for $k = [1, 2, \cdots, K]$, the received signal matrix of the k-th epoch can be written as:

$$\mathbf{X}[k] = \begin{bmatrix} \mathbf{x}[(k-1)N+1] & \cdots & \mathbf{x}[(k-1)N+N] \end{bmatrix} \in \mathbb{C}^{M\times N} \tag{3.24}$$

Concatenating the steering vectors of the k-th period into a matrix $\mathbf{A}[k]$, the complex amplitudes γ_ℓ into a diagonal matrix $\mathbf{\Gamma}[k]$ and the sampled and delayed C/A codes into a matrix $\mathbf{C}[k]$ the signal can be rewritten in a matrix notation. That is:

$$\mathbf{X}[k] = \mathbf{A}[k]\, \mathbf{\Gamma}[k]\, \mathbf{C}[k] + \mathbf{N}[k] \in \mathbb{C}^{M\times N} \tag{3.25}$$

Where: $\mathbf{A}_\ell = \begin{bmatrix} \mathbf{a}(\phi_1) & \cdots & \mathbf{a}(\phi_\ell) \end{bmatrix} \in \mathbb{C}^{M\times L}$ denotes the steering matrix of the k-th observation period. $\mathbf{\Gamma}[k] = \mathrm{diag}\{\gamma_\ell\} \in \mathbb{C}^{L\times L}$ is a diagonal matrix whose entries are the complex amplitudes of the signal. $\mathbf{C}[k] = \begin{bmatrix} \mathbf{c}[t-\tau_1] & \cdots & \mathbf{c}[t-\tau_\ell] \end{bmatrix}^{\mathrm{T}} \in \mathbb{C}^{L\times N}$ contains the sampled and delayed C/A codes.

Applying the vec{ } operator (see Appendix (A.4)) in the matrix $\mathbf{X}[k]$ in Equation (3.25), the following expression is obtained:

$$\mathrm{vec}\{\mathbf{X}[k]\} = \tilde{\mathbf{x}}[k] = (\mathbf{C}^{\mathrm{T}} \diamond \mathbf{A})\boldsymbol{\gamma}[k] + \tilde{\mathbf{n}}[k] \in \mathbb{C}^{MN\times 1} \tag{3.26}$$

Where the symbol $\diamond$ denotes the Khatri-Rao product (see Appendix (A.2)) and the vector $\boldsymbol{\gamma} = \begin{bmatrix} \gamma_1 & \cdots & \gamma_\ell \end{bmatrix} \in \mathbb{C}^{L\times K}$ contains the complex amplitudes related to each epoch. The index $[k]$ is omitted from the matrices $\mathbf{C}^{\mathrm{T}}$ and $\mathbf{A}$ due to the fact that they remain the same for every K period of collection of epochs.

Considering the K collected epochs in Equation (3.26), it is possible to obtain a matrix $\tilde{\mathbf{X}}$ by concatenating each $\tilde{\mathbf{x}}[k]$ vector into columns, such that:

$$\tilde{\mathbf{X}} = \begin{bmatrix} \tilde{\mathbf{x}}[1] & \cdots & \tilde{\mathbf{x}}[K] \end{bmatrix} \in \mathbb{C}^{MN \times K} \tag{3.27}$$

A matrix $\mathbf{\Gamma} = \begin{bmatrix} \boldsymbol{\gamma}[1] & \cdots & \boldsymbol{\gamma}[K] \end{bmatrix} \in \mathbb{C}^{L \times K}$ is defined as the concatenation of the complex amplitudes of each epoch. Then, from Equations (3.26) and (3.27) the matrix $\tilde{\mathbf{X}}$ can be rewritten as:

$$\tilde{\mathbf{X}} = (\mathbf{C}^{\mathrm{T}} \diamond \mathbf{A})\mathbf{\Gamma} + \tilde{\mathbf{N}} \in \mathbb{C}^{MN \times K} \tag{3.28}$$

$$\tilde{\mathbf{X}} = \tilde{\mathbf{X}}_0 + \tilde{\mathbf{N}} \in \mathbb{C}^{MN \times K} \tag{3.29}$$

Which is referred as the pre-correlation received signal matrix. In Equation (3.29) the term $\tilde{\mathbf{X}}_0 = (\mathbf{C}^{\mathrm{T}} \diamond \mathbf{A})\mathbf{\Gamma} \in \mathbb{C}^{MN \times K}$ is the noiseless received signal matrix. Notice that the transposed of $\tilde{\mathbf{X}}_0$ can be expressed as the first-mode reverse cyclical unfolding of a tensor $\boldsymbol{\mathcal{X}}_0$ (see Appendix (C.2)) as it follows:

$$\tilde{\mathbf{X}}_0^{\mathrm{T}} = \tilde{\mathbf{\Gamma}}^{\mathrm{T}}(\mathbf{C}^{\mathrm{T}} \diamond \mathbf{A})^{\mathrm{T}} = [\boldsymbol{\mathcal{X}}_0]_{(1)} \in \mathbb{C}^{K \times MN} \tag{3.30}$$

In such a way that the unfolding $[\boldsymbol{\mathcal{X}}_0]_{(1)}$ can be folded into the tensor $\boldsymbol{\mathcal{X}}_0$ which follows a Parallel Factor Analysis (PARAFAC) structure (see Appendix (C.4)). That is:

$$\boldsymbol{\mathcal{X}}_0 = \boldsymbol{\mathcal{I}}_{3,L} \times_1 \tilde{\mathbf{\Gamma}}^{\mathrm{T}} \times_2 \mathbf{C}^{\mathrm{T}} \times_3 \mathbf{A} \in \mathbb{C}^{K \times N \times M} \tag{3.31}$$

Where $\boldsymbol{\mathcal{I}}_{3,L} \in \mathbb{R}^{L \times L \times L}$ is denoted as the third-order identity tensor. Besides, the received pre-correlation signal presented in Equation (3.29) can be expressed in a tensor fashion such that:

$$\boldsymbol{\mathcal{X}} = \boldsymbol{\mathcal{X}}_0 + \boldsymbol{\mathcal{N}} \in \mathbb{C}^{K \times N \times M} \tag{3.32}$$

Hence, the term $\boldsymbol{\mathcal{N}} \in \mathbb{C}^{K \times N \times M}$ refers to the channel's AWGN characteristics, which can be expressed as a tensor.

3.4 Post-correlation signal model

As previously seen in Section (2.3.2) GNSS receivers perform a series of cross-correlations in order to align the incoming C/A code with the local generated replica. Towards conceiving this process, a bank of correlators, as presented in [15] [16], is employed to multiply the received signal with all possible shifted replicas for computing the cross-correlation vector necessary to estimate the time delay of the LOS component.

The correlator bank contains Q shifted signal replicas of a C/A code sequence $\mathbf{c}[t] \in \mathbb{R}^{1\times N}$ with corresponding time delay τ_q, where $q = \{1, \cdots, Q\}$, that is:

$$\mathbf{Q} = \begin{bmatrix} \mathbf{c}[t-\tau_1] & \cdots & \mathbf{c}[t-\tau_Q] \end{bmatrix}^{\mathrm{T}} \in \mathbb{R}^{N\times Q} \tag{3.33}$$

The correlation operation multiplies the received signal $\mathbf{X}$ in Equation (3.25) by the correlator bank $\mathbf{Q}$ in Equation (3.33). The result is referred as the post-correlation signal $\mathbf{Y}$. Therefore, for a given k-th epoch:

$$\mathbf{Y}[k] = \mathbf{X}[k]\mathbf{Q} \tag{3.34}$$

$$\mathbf{Y}[k] = \mathbf{A}[k]\,\mathbf{\Gamma}[k]\,\mathbf{C}[k]\mathbf{Q} + \mathbf{N}[k]\,\mathbf{Q} \in \mathbb{C}^{M\times Q} \tag{3.35}$$

Notice that in Equation (3.35) the term related to the noise becomes colored after being multiplied by the correlator bank. In order to avoid this issue, a Fisher information-preserving compression criterion [16] is applied to the bank $\mathbf{Q}$ by means of the economy-size Singular Value Decomposition (SVD) (see Appendix (A.6)) allowing to write:

$$\mathbf{Q} = \mathbf{U}\mathbf{\Sigma}\mathbf{V}^{\mathrm{H}} \tag{3.36}$$

Where $\mathbf{U} \in \mathbb{C}^{N\times Q}$, $\mathbf{\Sigma} \in \mathbb{C}^{Q\times Q}$ and $\mathbf{V} \in \mathbb{C}^{Q\times Q}$. The compressed correlator bank is defined as $\mathbf{Q}_\omega = \mathbf{U}$. Since it is an orthogonal and unitary matrix, when multiplied by the AWGN matrix $\mathbf{N}[k]$ the result preserves the statistical properties of the white Gaussian noise. Hence, the correlator bank in Equation (3.35) is replaced by the compressed correlator bank $\mathbf{Q}_\omega$ leading to:

$$\bar{\mathbf{Y}}[k] = \mathbf{A}[k]\,\mathbf{\Gamma}[k]\,\mathbf{C}[k]\,\mathbf{Q}_\omega + \mathbf{N}[k]\,\mathbf{Q}_\omega \tag{3.37}$$

$$\bar{\mathbf{Y}}[k] = \mathbf{A}[k]\,\mathbf{\Gamma}[k]\,\mathbf{C}[k]\,\mathbf{Q}_\omega + \mathbf{N}_\omega[k] \tag{3.38}$$

Where $\mathbf{N}_\omega[k]$ preserves white Gaussian noise's nature.

Notice that the signal model presented in Equation (3.38) has a similar structure regarding the model shown in Equation (3.25). Similarly as as performed from Equations (3.26) to (3.32), the post-correlation signal model can be expressed in a tensor fashion by:

$$\boldsymbol{\mathcal{Y}} = \boldsymbol{\mathcal{I}}_{3,L} \times_1 \mathbf{\Gamma}^{\mathrm{T}} \times_2 (\mathbf{C}\mathbf{Q}_\omega)^{\mathrm{T}} \times_3 \mathbf{A} + \boldsymbol{\mathcal{N}}_\omega \in \mathbb{C}^{K\times Q\times M} \tag{3.39}$$

The tensor-based signal model presented in Equation (3.39) has become subject of intensive research, worth mentioning [17] [18]. Since the purpose of this work is to deal with a tracking scenario, one state-of-the-art tensor-based time-delay estimation approach is presented. The technique is referred as the DoA/Khatri-Rao Factorization (DoA/KRF) [1] which has better performance and less computational complexity when compared to other solutions.

3.5 DoA Khatri-Rao Factorization - DoA/KRF

Since the post-correlation received signal model shown in Equation (3.39) follows a Parallel Factor Analysis (PARAFAC) model [2], DoA/KRF proposed in [1] estimates the model's factor matrices for later perform time-delay estimation. The approach starts by reconstructing the array steering factor matrix through an ESPRIT-DoA estimation technique presented in Subsection (3.5.1), the remaining factor matrices are then obtained by means of the Khatri-Rao factorization (KRF) [19] shown in Subsection (3.5.2). Later, the time-delay estimation is performed via the signal's greatest power approach, pointed in subsection (3.5.3).

In order to perform DoA estimation on the received signal tensor, the array steering matrix $\mathbf{A} \in \mathbb{C}^{M \times N}$ must be exposed in a similar fashion as the signal model seen previously on Equation (3.21). Hence, the received signal tensor is unfolded into its third-mode reverse cyclical unfolding, given by:

$$[\boldsymbol{\mathcal{Y}}]_{(3)} = \mathbf{A}\left(\boldsymbol{\Gamma}^{\mathrm{T}} \diamond (\mathbf{C}\mathbf{Q}_{\omega})^{\mathrm{T}}\right)^{\mathrm{T}} + \mathbf{N}_{\omega} \in \mathbb{C}^{M \times KQ} \tag{3.40}$$

3.5.1 Estimation of Signal Parameter via Rotational Invariance Technique - ESPRIT

Proposed in [14] as a subspace-based method for DoA estimation, ESPRIT provides a closed-form solution with low computational complexity. First, the Eigenvalue Decomposition (EVD) is applied on the estimated received signal covariance matrix (see Appendix (B.1)), such that:

$$\hat{\mathbf{R}} = \mathbf{U}\boldsymbol{\Sigma}\mathbf{U}^{\mathrm{H}} \in \mathbb{C}^{M \times M} \tag{3.41}$$

Where $\mathbf{U} \in \mathbb{C}^{M \times M}$ denotes the matrix of the signal's eigenvectors and $\boldsymbol{\Sigma} \in \mathbb{C}^{M \times M}$ is a diagonal matrix containing the signal's eigenvalues.

Since the L number of received signals by the Vandermonde left centro-hermitian ULA is considered to be known, the signal subspace matrix can be obtained through a low-rank approximation by selecting the first L columns of $\mathbf{U}$ that is:

$$\mathbf{U} = \left[\mathbf{U}_s | \mathbf{U}_n\right] \in \mathbb{C}^{M \times M} \tag{3.42}$$

Where $\mathbf{U}_s \in \mathbb{C}^{M \times l}$ is the signal subspace matrix and $\mathbf{U}_n \in \mathbb{C}^{M \times (M-l)}$ is the subspace related to the noise. Now considering that the number of antenna elements M in the ULA is greater than the number of L received signals, the shift invariance equation expressed below can be solved.

$$\mathbf{J}_1\mathbf{A}\boldsymbol{\Phi} = \mathbf{J}_2\mathbf{A} \tag{3.43}$$

Where $\mathbf{A} \in \mathbb{C}^{M \times l}$ is the steering matrix presented before in Equation (3.52), $\mathbf{J}_1 = [\mathbf{I}_M \;\; 0_{M\times 1}] \in \mathbf{C}^{M-1\times M}$ and $\mathbf{J}_2 = [0_{M\times 1} \;\; \mathbf{I}_M] \in \mathbf{C}^{M-1\times M}$ are selection matrices.

Since the matrix $\mathbf{A}$ can be re-obtained by multiplying the matrix $\mathbf{U}_s$ by a transformation matrix $\mathbf{T}$ such that $\mathbf{A} = \mathbf{U}_s\mathbf{T}$, the Equation (3.43) becomes:

$$\mathbf{J}_1\mathbf{U}_s\mathbf{T}\mathbf{\Phi} = \mathbf{J}_2\mathbf{U}_s\mathbf{T} \tag{3.44}$$

Applying the Moore-Penrose pseudoinverse operator in term $\mathbf{J}_1\mathbf{U}_s$ in Equation (3.44) and multiplying by $\mathbf{T}^+$, the shift invariance equation can be rewritten as:

$$\mathbf{T}\mathbf{\Phi}\mathbf{T}^+ = (\mathbf{J}_1\mathbf{U}_s)^+\mathbf{J}_2\mathbf{U}_s \tag{3.45}$$

By defining $\mathbf{\Psi} = \mathbf{T}\mathbf{\Phi}\mathbf{T}$ as a matrix which contains information about the spatial frequencies, it is possible to apply EVD in $\mathbf{\Psi}$ obtaining:

$$\mathbf{\Psi} = \mathbf{\Sigma}\mathbf{\Lambda}\mathbf{\Sigma}^{\mathrm{H}} \tag{3.46}$$

Where $\mathbf{\Lambda} \in \mathbb{C}^{l\times l}$ is a diagonal matrix of interest which contains the desired spatial frequencies $e^{j\mu_\ell}$, that is:

$$\mathrm{diag}\{\mathbf{\Lambda}\} = \left[e^{j\mu_1}, \cdots, e^{j\mu_\ell}\right] \tag{3.47}$$

The estimated spatial frequencies are given by:

$$\hat{\mu}_\ell = \arg\{e^{j\mu_\ell}\} \tag{3.48}$$

And the corresponding angles of arrival can be expressed as:

$$\theta_\ell = \arcsin\left(-\frac{\lambda}{2\pi\Delta}\hat{\mu}_\ell\right) \tag{3.49}$$

Considering that each antenna element is equally spaced in such a way that their distance matches the received signal's wavelength, i.e. $\Delta = \lambda$, the Equation (3.49) becomes:

$$\theta_\ell = \arcsin\left(-\frac{1}{2\pi}\hat{\mu}_\ell\right) \tag{3.50}$$

In order to apply ESPRIT in a highly multipath environment, decorrelating methods are necessary for multipath mitigation. Thus, the techniques Forward-Backward Averaging (FBA) [20] and Expanded Spatial Smoothing (ESPS) [21] [22] are applied on the received signal model.

Algorithm 1 DoA estimation via ESPRIT [14]

1. Initialization:
   1.1 – Define the selection matrices $\mathbf{J_1}$ and $\mathbf{J_2}$.
   $\mathbf{J_1} = [\mathbf{I}_M \;\; 0_{M\times 1}]$
   $\mathbf{J_2} = [0_{M\times 1} \;\; \mathbf{I}_M]$

2. Obtain an estimation for the signal subspace.
   $\hat{\mathbf{U}}_\mathbf{s} = \text{EVD}\,(\mathbf{R}_{xx})$

3. Solve the shift invariance equation to obtain an estimation for $\mathbf{\Psi}$.
   $\hat{\mathbf{\Psi}} = (\mathbf{J}_1\hat{\mathbf{U}}_\mathbf{s})^{+}\mathbf{J}_2\hat{\mathbf{U}}_\mathbf{s}$

3. Obtain an estimation for the spatial frequencies $\hat{\mu}_\ell$.
   $\{\hat{\mu}_\ell\} = \text{diag}\left\{\text{EIG}\left(\hat{\mathbf{\Psi}}\right)\right\}$

4. Find the corresponding angles of arrival $\hat{\theta}_\ell$.
   $\{\hat{\theta}_\ell\} = \arcsin\left(-\frac{1}{2\pi}\{\hat{\mu}_\ell\}\right)$

Table 4 – Summary of the ESPRIT algorithm.

3.5.2 Estimation of the factor matrices

As seen in Subsection (3.5.1) ESPRIT provides an estimation for the angle of arrival of the L received signals. Since the carrier frequency and array response are known, it is possible to estimate each steering vector $\hat{\mathbf{a}}(\theta_\ell)$ related to the array steering factor matrix $\hat{\mathbf{A}} \in \mathbb{C}^{M\times L}$ such that:

$$\hat{\mathbf{a}}(\hat{\theta}_\ell) = \begin{bmatrix} 1 & e^{j\hat{\theta}_\ell} & \cdots & e^{j(m-1)\hat{\theta}_\ell} \end{bmatrix} \in \mathbb{C}^{1\times M} \tag{3.51}$$

By concatenating the L estimated steering vectors, an estimation for the array steering factor matrix is obtained:

$$\hat{\mathbf{A}}(\theta_\ell) = \begin{bmatrix} \mathbf{a}(\theta_1) & \cdots & \mathbf{a}(\theta_\ell) \end{bmatrix}^{\mathrm{T}} \in \mathbb{C}^{M\times L} \tag{3.52}$$

Once $\hat{\mathbf{A}} \in \mathbb{C}^{M\times L}$ is reconstructed, its pseudo-inverse can be applied to (3.40) leading to:

$$\hat{\mathbf{A}}^{+}\,[\boldsymbol{\mathcal{Y}}]_{(3)} = \hat{\mathbf{A}}^{+}\mathbf{A}\left(\mathbf{\Gamma}^{\mathrm{T}} \diamond (\mathbf{C}\mathbf{Q}_\omega)^{\mathrm{T}}\right)^{\mathrm{T}} \tag{3.53}$$

$$\hat{\mathbf{A}}^{+}\,[\boldsymbol{\mathcal{Y}}]_{(3)} \approx \left(\mathbf{\Gamma}^{\mathrm{T}} \diamond (\mathbf{C}\mathbf{Q}_\omega)^{\mathrm{T}}\right)^{\mathrm{T}} \in \mathbb{C}^{L\times KQ} \tag{3.54}$$

Notice that the transposed of the output of Equation (3.54) results in:

$$\left[\hat{\mathbf{A}}^{+}\,[\boldsymbol{\mathcal{Y}}]_{(3)}\right]^{\mathrm{T}} \approx \left(\mathbf{\Gamma}^{\mathrm{T}} \diamond (\mathbf{C}\mathbf{Q}_\omega)^{\mathrm{T}}\right) \in \mathbb{C}^{KQ\times L} \tag{3.55}$$

Which is the Khatri-Rao product between the factor matrices $\mathbf{\Gamma}^{\mathrm{T}} \in \mathbb{C}^{K\times L}$ and $(\mathbf{C}\mathbf{Q}_{\omega})^{\mathrm{T}}\,\mathbb{C}^{Q\times L}$. By means of the Least-Squares Khatri-Rao factorization (see Appendix (A.7)) the remaining factor matrices can be estimated. Considering each ℓ column of the output of Equation (3.54) as:

$$\left(\mathbf{\Gamma}^{\mathrm{T}} \diamond (\mathbf{C}\mathbf{Q}_{\omega})^{\mathrm{T}}\right)_{(:,\,\ell)} \in \mathbb{C}^{KQ\times 1} \tag{3.56}$$

Which can be reshaped into a matrix:

$$\underset{Q\times K}{\mathrm{unvec}}\left\{\left(\mathbf{\Gamma}^{\mathrm{T}} \diamond (\mathbf{C}\mathbf{Q}_{\omega})^{\mathrm{T}}\right)_{(:,\,\ell)}\right\} = (\mathbf{C}\mathbf{Q}_{\omega})^{\mathrm{T}}_{(:,\,\ell)}\,(\mathbf{\Gamma}^{\mathrm{T}}_{(:,\,\ell)})^{\mathrm{T}} \in \mathbb{C}^{Q\times K} \tag{3.57}$$

The result obtained in Equation (3.57) corresponds to a vectorized representation of a rank-1 matrix. Applying a SVD-based rank-one approximation yields:

$$\underset{Q\times K}{\mathrm{unvec}}\left\{\left(\mathbf{\Gamma}^{\mathrm{T}} \diamond (\mathbf{C}\mathbf{Q}_{\omega})^{\mathrm{T}}\right)_{(:,\,\ell)}\right\} = \mathbf{u}_{\ell}\,\sigma_{\ell}\,\mathbf{v}_{\ell}^{\mathrm{H}} \in \mathbb{C}^{Q\times K} \tag{3.58}$$

An estimation for the l-th column of each factor matrix is obtained by taking the square root of the singular value in Equation (3.58) according to:

$$\tilde{\mathbf{\Gamma}}^{\mathrm{T}}_{(:,\,\ell)} = \mathbf{v}_{\ell}^{*}\sqrt{\sigma}_{\ell} \tag{3.59}$$

$$\left(\mathbf{C}\tilde{\mathbf{Q}}_{\omega}\right)^{\mathrm{T}}_{(:,\,\ell)} = \mathbf{u}_{\ell}\sqrt{\sigma}_{\ell} \tag{3.60}$$

The factor matrices are then rebuild by repeating the procedure from Equations (3.56) to (3.60) for all L columns.

3.5.3 Time delay estimation

When realizing the procedure shown in Equation (3.54) occurrence of permutation ambiguities is possible due to the order of concatenation of the estimated steering vectors of Equation (3.52). In this scenario, the estimated factor matrix $\left(\mathbf{C}\tilde{\mathbf{Q}}_{\omega}\right)^{\mathrm{T}} \in \mathbb{C}^{Q\times L}$ may present its L columns permuted. To find which row corresponds to the LOS component, the greatest power based scheme approach [1] is considered.

Assuming that received signal LOS component has the greatest signal power in comparison with the NLOS replicas, the following expression can be used to locate the column index of the LOS component:

$$l_{\mathrm{LOS}} = \max_{\ell} ||\tilde{\mathbf{\Gamma}}^{\mathrm{T}}_{(:,\,\ell)}||_2 \tag{3.61}$$

Where $\tilde{\mathbf{\Gamma}}^{\mathrm{T}}_{(:,\,l)}$ is the l-th column of the estimated factor matrix $\tilde{\mathbf{\Gamma}}^{\mathrm{T}} \in \mathbb{C}^{K\times L}$ and $||\ \ ||_2$ is the vector norm operator. The Equation (3.61) provides a column index l_{LOS} to be selected in the matrix $\left(\mathbf{C}\tilde{\mathbf{Q}}_{\omega}\right)^{\mathrm{T}} \in \mathbb{C}^{Q\times L}$ such that:

$$\hat{\mathbf{c}}_{\mathrm{LOS}} = \left(\mathbf{C}\tilde{\mathbf{Q}}_{\omega}\right)^{\mathrm{T}}_{(:,\,\ell_{\mathrm{LOS}})} \in \mathbb{C}^{Q\times 1} \tag{3.62}$$

Then, an output for the correlator bank is computed by:

$$\mathbf{q}_{\text{DoA/KRF}} = \hat{\mathbf{c}}_{\text{LOS}}\, \boldsymbol{\Sigma}\, \mathbf{V}^{\text{H}} \in \mathbb{C}^{Q\times 1} \tag{3.63}$$

The time-delay estimation is obtained by verifying the cross-correlation values of $\mathbf{q}_{\text{DoA/KRF}}$ in Equation (3.63). For this, a cubic spline interpolation based on $|\mathbf{q}_{\text{DoA/KRF}}|$ is used to generate a cost function $F(\tau)$ such that the τ variable that maximizes the cost function will be the estimated time-delay for the LOS signal component, such that:

$$\hat{\tau}_{LOS} = \arg\max_{\tau}\{F(\tau)\} \tag{3.64}$$

The DoA/KRF Time-delay estimation algorithm is summarized in Table (5).

Algorithm 2 DoA/KRF Time-delay estimation [1]

1. ESPRIT main section: Table (4). Estimate the angle of arrival of the L received signals.
   $\{\hat{\theta}_\ell\} = \text{ESPRIT}\left([\boldsymbol{\mathcal{Y}}]_{(3)}\right)$

2. Obtain each steering vector $\hat{\mathbf{a}}(\theta_\ell)$ related to the array steering factor matrix.
   `for` $\ell = 1, \ldots, L$ `do:`
   $\hat{\mathbf{a}}(\hat{\theta}_\ell) = \begin{bmatrix} 1 & e^{j\hat{\theta}_\ell} & \cdots & e^{j(m-1)\hat{\theta}_\ell} \end{bmatrix}$
   `end`

3. Rebuild the array steering factor matrix.
   $\hat{\mathbf{A}}(\theta_\ell) = \begin{bmatrix} \mathbf{a}(\theta_1) & \cdots & \mathbf{a}(\theta_\ell) \end{bmatrix}^{\mathrm{T}}$

4. Obtain an estimation for the Khatri-Rao product.
   $\left(\boldsymbol{\Gamma}^{\mathrm{T}} \diamond (\mathbf{C}\mathbf{Q}_\omega)^{\mathrm{T}}\right) = \text{transpose}\left\{\hat{\mathbf{A}}^{+}\,[\boldsymbol{\mathcal{Y}}]_{(3)}\right\}$

5. Estimate the remaining factor matrices by means of the Khatri-Rao factorization.
   `for` $\ell = 1, \ldots, L$ `do:`
   $\underset{Q\times K}{\text{unvec}}\left\{\left(\boldsymbol{\Gamma}^{\mathrm{T}} \diamond (\mathbf{C}\mathbf{Q}_\omega)^{\mathrm{T}}\right)_{(:,\,\ell)}\right\} = (\mathbf{C}\mathbf{Q}_\omega)^{\mathrm{T}}_{(:,\,\ell)}\,(\boldsymbol{\Gamma}^{\mathrm{T}}_{(:,\,\ell)})^{\mathrm{T}}$
   $\text{SVD}\left\{(\mathbf{C}\mathbf{Q}_\omega)^{\mathrm{T}}_{(:,\,\ell)}\,(\boldsymbol{\Gamma}^{\mathrm{T}}_{(:,\,\ell)})^{\mathrm{T}}\right\} = \mathbf{u}_\ell\,\sigma_\ell\,\mathbf{v}_\ell^{\mathrm{H}}$
   $\hat{\boldsymbol{\Gamma}}^{\mathrm{T}}_{(:,\,\ell)} = \mathbf{v}^{*}_{\ell}\sqrt{\sigma}_\ell$
   $\left(\mathbf{C}\hat{\mathbf{Q}}_\omega\right)^{\mathrm{T}}_{(:,\,\ell)} = \mathbf{u}_\ell\sqrt{\sigma}_\ell$
   `end`

6. With $\hat{\boldsymbol{\Gamma}}^{\mathbf{T}}$ and $\left(\mathbf{C}\hat{\mathbf{Q}}_\omega\right)^{\mathrm{T}}$ perform the time-delay estimation.
   `for` $\ell = 1, \ldots, L$ `do:`
   $\{\ell_{\text{index}}\} = ||\tilde{\boldsymbol{\Gamma}}^{\mathrm{T}}_{(:,\,\ell)}||_2$
   `end`
   $\ell_{\text{LOS}} = \max_{\ell}\{\ell_{\text{index}}\}$
   $\hat{\mathbf{c}}_{\text{LOS}} = \left(\mathbf{C}\hat{\mathbf{Q}}_\omega\right)^{\mathrm{T}}_{(:,\,\ell_{\text{LOS}})}$
   $\mathbf{q}_{\text{DoA/KRF}} = \hat{\mathbf{c}}_{\text{LOS}}\,\boldsymbol{\Sigma}\,\mathbf{V}^{\mathrm{H}}$
   $\hat{\tau}_{LOS} = \arg\max_{\tau}\{F(\tau)\}$

Table 5 – Summary of the DoA/KRF algorithm.

4 Tensor-based Tracking Approaches

4.1 Introduction

As seen on Chapter [3] on Section (3.5) the presented tensor-based technique for time-delay estimation rely on collecting K received signal epochs to later perform estimations. This process is named as the batch-mode approach, which is illustrated on Figure (12) where $\boldsymbol{\mathcal{Y}}_n = \{1, \ldots, n, \ldots, N\}$ is a group of N observed tensors. In this context, considering a real-time tracking scenario, the computation of a full EVD/SVD at every sampling instant is not suitable, due to complexity reasons [23]. Therefore, an alternative to reduce the Time of Computing (ToC) of subspace estimations has been the development of subspace tracking algorithms [24].

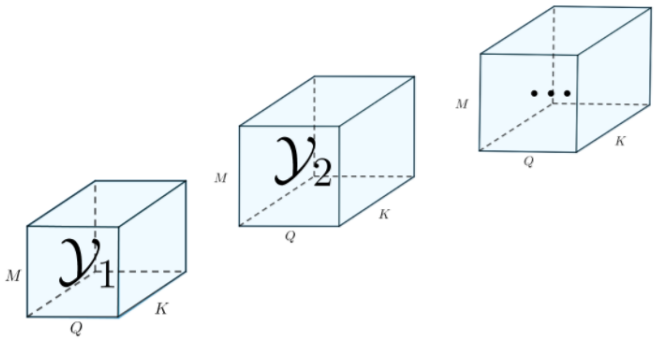

Figure 12 – Illustration of the observed tensors in the batch-mode approach.

Another issue that should be mentioned is that for a given K collection of epochs, some column vectors of sequential data samples may be composed of different time-delay and direction of arrival parameters, which leads to imprecise estimates. Thus, each serially acquired data must be weighted in such a way that the most recent acquisitions are strengthen when compared to past observations. Figure (13) shows this process:

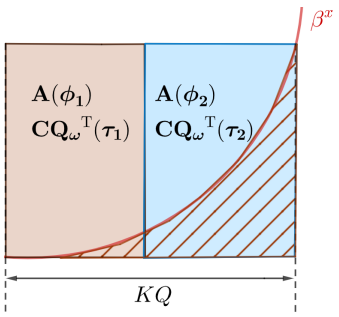

Figure 13 – Illustration of an weighting exponential β^x applied to the observed data.

4.2 Statement of the problem

The problem states that a sequence of N observed tensors expressed in Figure (12) are serially acquired by means of their epochs. Each acquisition corresponds to a matrix to be concatenated into the dimension K of the previously observed data. Figure (14) illustrates this process.

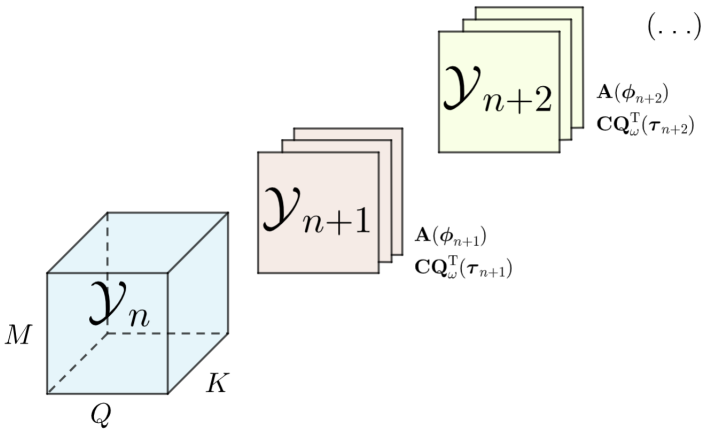

Figure 14 – Observed epochs being concatenated to the dimension K of previously observed data.

The concatenation process results in a third-order tensor of which one dimension increases with time while the other two dimensions remain fixed. The resulting tensor can be expressed as:

$$\boldsymbol{\mathcal{Y}} = [\boldsymbol{\mathcal{Y}}_1 \,|\, \boldsymbol{\mathcal{Y}}_2 \,|\, \ldots \,|\, \boldsymbol{\mathcal{Y}}_n \,|\, \ldots \,|\, \boldsymbol{\mathcal{Y}}_N] \in \mathbb{C}^{K\,(1+\cdots+n+\cdots+N)\times Q\times M} \tag{4.1}$$

For the sake of simplicity, each factor matrix associated with its n-th tensor will be referred as a n-th index element of a sequence of N factor matrices, such that the following sequences:

$$\mathbf{A}[\boldsymbol{\phi}] = \{\mathbf{A}[\phi_1] \quad \ldots \quad \mathbf{A}[\phi_n] \quad \ldots \quad \mathbf{A}[\phi_N]\} \tag{4.2}$$

$$(\mathbf{CQ}_{\omega})^{\mathrm{T}}[\boldsymbol{\tau}] = \{(\mathbf{CQ}_{\omega})^{\mathrm{T}}[\tau_1] \quad \ldots \quad (\mathbf{CQ}_{\omega})^{\mathrm{T}}[\tau_n] \quad \ldots \quad (\mathbf{CQ}_{\omega})^{\mathrm{T}}[\tau_N]\} \tag{4.3}$$

$$\boldsymbol{\Gamma}^{\mathrm{T}}[\mathbf{n}] = \{\boldsymbol{\Gamma}^{\mathrm{T}}[1] \quad \ldots \quad \boldsymbol{\Gamma}^{\mathrm{T}}[n] \quad \ldots \quad \boldsymbol{\Gamma}^{\mathrm{T}}[N]\} \tag{4.4}$$

Represent all factor matrices associated to each upcoming received signal tensor as seen on Equation (3.39). For instance, the n-th observed tensor can be expressed as:

$$[\boldsymbol{\mathcal{Y}}_n]_{(3)} = \boldsymbol{\mathcal{I}}_{3,L} \times_1 \boldsymbol{\Gamma}^{\mathrm{T}}[n] \times_2 (\mathbf{CQ}_{\omega})^{\mathrm{T}}[\tau_n] \times_3 \mathbf{A}[\phi_n] + \boldsymbol{\mathcal{N}}_{\omega} \in \mathbb{C}^{K\times Q\times M} \tag{4.5}$$

In order to perform time-delay estimation on Equation (4.1) we consider the problem of tracking the PARAFAC decomposition of each upcoming third-order tensor. In other words, at a given time instant, each factor matrix associated to the current observed tensor must be estimated. In addition, the influence of past observations must be suppressed.

4.3 Tracking scenario

This section presents the data model for the tracking scenario, which takes into account the problems stated on the previous section. The derivation begins by reducing the influence of past observations, which is done by applying a sliding window of length K to the current data such that the output tensor will have dimensions $\mathbb{C}^{K\times Q\times M}$ as illustrated on Figure (15).

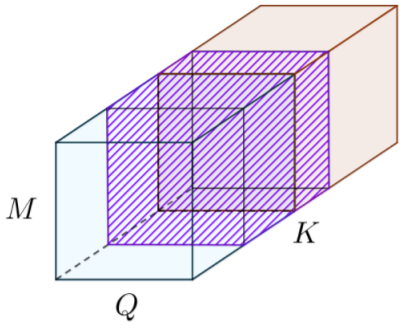

Figure 15 – Resulting tensor (illustrated in purple) after applying a sliding window of length K.

Since the estimates are performed on the observed tensor's third-mode unfolding, the tensor provided by the sliding window is unfolded into a matrix of dimensions $\mathbb{C}^{M\times KQ}$ as seen on Equation (3.40) which in most of the cases will be composed of past observations denoted as $(n-1)$ and present contributions referred as (n). This setting is exposed in Figure (16).

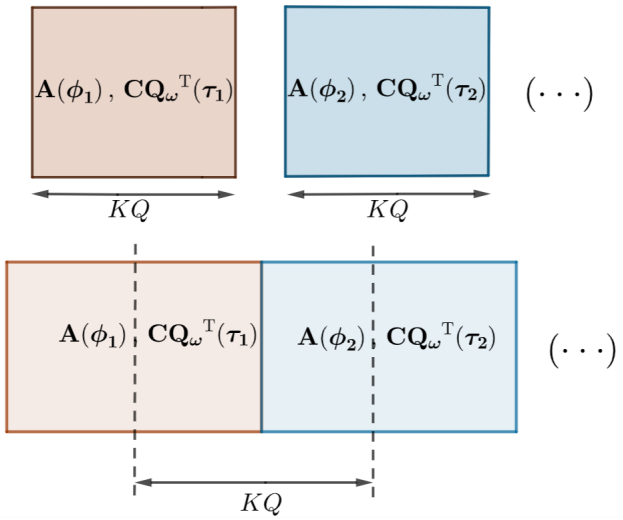

Figure 16 – Unfolding perspective of the applied sliding window. Notice that the length of the window changes to KQ.

The tracking scenario assumes at a given time instant (t) the existence of a previously analyzed data matrix $[\boldsymbol{\mathcal{Y}}]_{(3)}(t) \in \mathbb{C}^{M\times KQ}$. For instance, we will take $\boldsymbol{\mathcal{Y}}_1$ from Equation (4.1). Its third-mode unfolding $[\boldsymbol{\mathcal{Y}}_1]_{(3)}$ is expressed as:

$$[\boldsymbol{\mathcal{Y}}]_{(3)}(t) = [\boldsymbol{\mathcal{Y}}_1]_{(3)} = \mathbf{A}[\phi_1]\left(\boldsymbol{\Gamma}^{\mathrm{T}}[1] \diamond (\mathbf{C}\mathbf{Q}_{\omega})^{\mathrm{T}}[\tau_1]\right)^{\mathrm{T}} + \mathbf{N}_{\omega} \in \mathbb{C}^{M\times KQ} \tag{4.6}$$

At time instant $(t+1)$ an upcoming epoch from $\boldsymbol{\mathcal{Y}}_2$ is received, that is:

$$[\boldsymbol{\mathcal{Y}}_2]_{(3)_{\uparrow Q}} = \mathbf{A}[\phi_2]\left(\boldsymbol{\Gamma}^{\mathrm{T}}_{\rightarrow 1}[2] \diamond (\mathbf{C}\mathbf{Q}_{\omega})^{\mathrm{T}}[\tau_2]\right)^{\mathrm{T}} \in \mathbb{C}^{M\times Q} \tag{4.7}$$

Where $\boldsymbol{\Gamma}^{\mathrm{T}}_{\rightarrow 1}[2] \in \mathbb{C}^{1\times L}$ selects the first row vector from $\boldsymbol{\Gamma}^{\mathrm{T}}[2]$ in Equation (4.4). The observed epoch is appended to Equation (4.6) according to:

$$[\boldsymbol{\mathcal{Y}}]_{(3)}(t+1) = \begin{bmatrix}[\boldsymbol{\mathcal{Y}}_1]_{(3)_{\downarrow Q}} & [\boldsymbol{\mathcal{Y}}_2]_{(3)_{\uparrow Q}}\end{bmatrix} \in \mathbb{C}^{M\times KQ} \tag{4.8}$$

Where $[\boldsymbol{\mathcal{Y}}_1]_{(3)_{\downarrow Q}} \in \mathbb{C}^{M\times(K-1)Q}$ suppresses the first Q columns of $[\boldsymbol{\mathcal{Y}}_1]_{(3)}$ related to the oldest observed epoch. The process is repeated for $t = (1, 2, \ldots, (N-1)K)$ such that the following expressions:

$$[\boldsymbol{\mathcal{Y}}]_{(3)}(t) = [\boldsymbol{\mathcal{Y}}_1]_{(3)} \in \mathbb{C}^{M\times KQ} \tag{4.9}$$
$$[\boldsymbol{\mathcal{Y}}]_{(3)}(t+1) = \begin{bmatrix}[\boldsymbol{\mathcal{Y}}_1]_{(3)_{\downarrow Q}} & [\boldsymbol{\mathcal{Y}}_2]_{(3)_{\uparrow Q}}\end{bmatrix} \in \mathbb{C}^{M\times KQ} \tag{4.10}$$
$$[\boldsymbol{\mathcal{Y}}]_{(3)}(t+2) = \begin{bmatrix}[\boldsymbol{\mathcal{Y}}_1]_{(3)_{\downarrow 2*Q}} & [\boldsymbol{\mathcal{Y}}_2]_{(3)_{\uparrow 2*Q}}\end{bmatrix} \in \mathbb{C}^{M\times KQ} \tag{4.11}$$
$$\vdots \tag{4.12}$$
$$[\boldsymbol{\mathcal{Y}}]_{(3)}(t+K) = \begin{bmatrix}[\boldsymbol{\mathcal{Y}}_2]_{(3)}\end{bmatrix} \in \mathbb{C}^{M\times KQ} \tag{4.13}$$
$$[\boldsymbol{\mathcal{Y}}]_{(3)}(t+K+1) = \begin{bmatrix}[\boldsymbol{\mathcal{Y}}_2]_{(3)_{\downarrow Q}} & [\boldsymbol{\mathcal{Y}}_3]_{(3)_{\uparrow Q}}\end{bmatrix} \in \mathbb{C}^{M\times KQ} \tag{4.14}$$
$$[\boldsymbol{\mathcal{Y}}]_{(3)}(t+K+2) = \begin{bmatrix}[\boldsymbol{\mathcal{Y}}_2]_{(3)_{\downarrow 2*Q}} & [\boldsymbol{\mathcal{Y}}_3]_{(3)_{\uparrow 2*Q}}\end{bmatrix} \in \mathbb{C}^{M\times KQ} \tag{4.15}$$
$$\vdots \tag{4.16}$$
$$[\boldsymbol{\mathcal{Y}}]_{(3)}(t+2K) = \begin{bmatrix}[\boldsymbol{\mathcal{Y}}_3]_{(3)}\end{bmatrix} \in \mathbb{C}^{M\times KQ} \tag{4.17}$$
$$[\boldsymbol{\mathcal{Y}}]_{(3)}(t+2K+1) = \begin{bmatrix}[\boldsymbol{\mathcal{Y}}_3]_{(3)_{\downarrow 2*Q}} & [\boldsymbol{\mathcal{Y}}_4]_{(3)_{\uparrow 2*Q}}\end{bmatrix} \in \mathbb{C}^{M\times KQ} \tag{4.18}$$
$$\vdots \tag{4.19}$$
$$[\boldsymbol{\mathcal{Y}}]_{(3)}(t+(N-1)K) = \begin{bmatrix}[\boldsymbol{\mathcal{Y}}_N]_{(3)}\end{bmatrix} \in \mathbb{C}^{M\times KQ} \tag{4.20}$$

Represent the tracking scenario over time. Notice that at each time instant, the resulting data has dimensions $\mathbb{C}^{M\times KQ}$ which corresponds to the third-mode unfolding of the output tensor of the sliding window of length K. For instance, Figure (17) illustrates the concatenation process for a given time instant $(t+1)$ between the n-th and the subsequent $n+1$-th observed tensor.

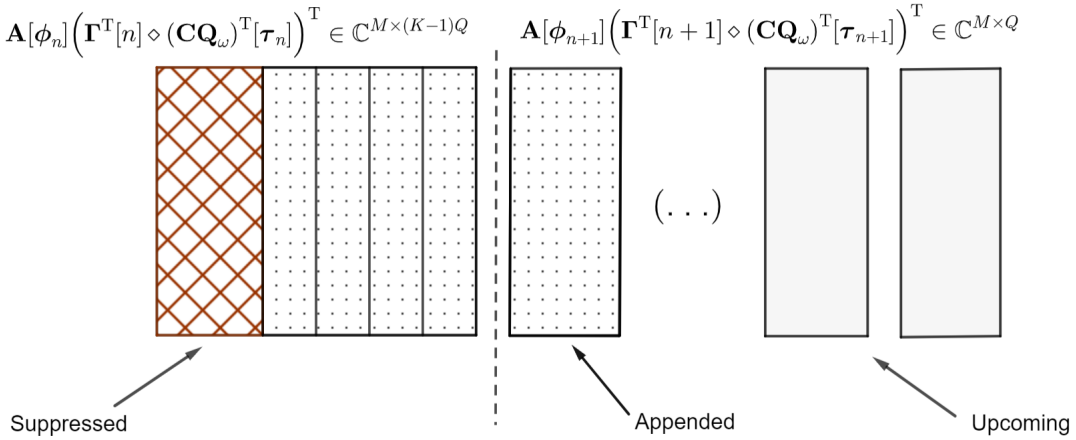

Figure 17 – Process of appending an upcoming observation at time instant $(t+1)$.

In order to perform DoA/KRF on Equations (4.9) to (4.20) instead of applying an SVD at each upcoming epoch to obtain an estimation for the signal subspace $\mathbf{U}_s(t+1) \in \mathbb{C}^{M\times L}$, a subspace tracking technique based on the past observation $\mathbf{U}_s(t)$ can be employed. The objective is to decide for a low computational complexity technique which must also provide a high convergence rate to $\mathbf{U}_s(t+1)$. In this sense, this work proposes a subspace tracker to be added to the DoA/KRF technique. Figure (18) presents the resulting block diagram of the proposed approach.

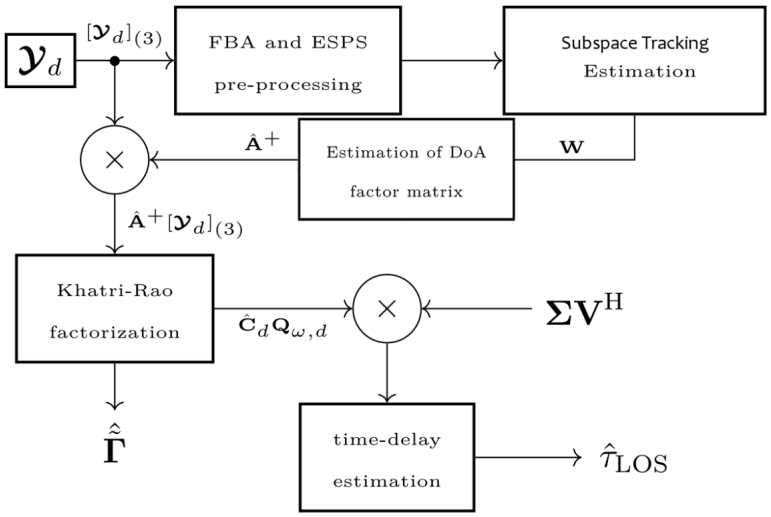

Figure 18 – Block diagram of the proposed subspace tracking estimator to be added to the DoA/KRF technique. Figure adapted from [1].

When selecting a subspace tracking algorithm for a desired application, the scenario under consideration must be discussed. The reader may refer to [25] for an exhaustive literature review of the current state-of-the-art techniques. This work focus on the class of the low complexity methods [26], which are the most important ones from a real time implementation point of view.

Before start to detail the selected techniques, some considerations regarding the behaviour of the data during the tracking scenario are assumed:

- The direction of arrival and time-delay parameters have a smooth variation between each collected epoch. There are no sudden changes on the received signal.
- For ESPRIT-based DoA estimation, only a small part of the eigenstructure of the estimated signal subspace is sufficient. There is no need to compute an orthornomal subspace basis at each time step. [24] [26]
- Tracking the eigenvalues is not necessary.

Throughout the Sections (4.4) and (4.6) the selected subspace tracking methods are described. Their implementation on the DoA/KRF time-delay estimation technique is presented on Sections (4.5) and (4.7). Later, the review of the computational complexity of the proposed techniques is discussed on Section (4.8).

4.4 Projection Approximation Subspace Tracking - PAST

The PAST algorithm proposed by [27] derives from the minimization of the linear Principal Component Analysis (PCA) criterion [28] which is a measure for the correlation between sequential observed data snapshots $\{\mathbf{x}(n)\}$ and is a reference for signal subspace interpretation. The expression is defined as:

$$J(\mathbf{U}_s(n)) = \mathrm{E}\{\, ||\mathbf{x}(n) - \mathbf{U}(n)\mathbf{U}(n)^{\mathrm{H}}\mathbf{x}(n)||_F^2 \,\} \tag{4.21}$$

Which has a global minimum when $\mathbf{U}(n)$ is equal to the signal subspace basis of the covariance matrix of each observed data vector $\{\mathbf{x}(n)\}$. In this circumstance, $\mathbf{x}(n)$ and its projection $\mathbf{U}(n)\mathbf{U}(n)^{\mathrm{H}}\mathbf{x}(n)$ into the signal subspace are most similar.

In order to provide a solution for Equation (4.21) the expectation operator is replaced by an exponentially weighted sum over n samples and the projection term $\mathbf{U}(n)^{\mathrm{H}}\mathbf{x}(n)$ is rewritten by means of its previous estimation $\mathbf{U}(n-1)^{\mathrm{H}}\mathbf{x}(n)$ leading to the following cost function to me minimized:

$$J'(\mathbf{U}_s(n)) = \sum_{i=1}^{t} \beta^{t-i} ||\mathbf{x}(n) - \mathbf{U}_s(n)\mathbf{U}_s(n-1)^{\mathrm{H}}\mathbf{x}(n)||_F^2 \tag{4.22}$$

Where $\beta < 1$ is referred as the forgetting factor, $\mathbf{U}_s(n)$ is the signal subspace estimation at a given time instant (n) and $\{\mathbf{x}(n)\}$ is a sequence of n observed data vectors. After manipulation [27], the minimization of Equation (4.22) is given by a series of recursive updates for the estimation of the signal subspace $\mathbf{U}_s(n)$. The result provides a computational complexity of $\mathcal{O}(Nl)$ instead of $\mathcal{O}(N^3)$ operations for a full EVD. The pseudo-code of the technique is presented in Table (6).

Algorithm 3 Projection Approximation Subspace Tracking - PAST [27]

1. Initialization:
   $\mathbf{P}(0) = \mathbf{I}_R$
   $\hat{\mathbf{U}}_\mathbf{s}(0) = \mathbf{I}_{M\times R}$

2. PAST main section:
   `for` $n = 1, 2, \ldots$ `do:`
   $\mathbf{y}(n) = \hat{\mathbf{U}}_\mathbf{s}^{\mathrm{H}}(n-1)\,\mathbf{x}(n)$
   $\mathbf{h}(n) = \mathbf{P}(n-1)\,\mathbf{y}(n)$
   $\mathbf{g}(n) = \mathbf{h}(n-1)/\left(\beta + \mathbf{y}^{\mathrm{H}}(n)\,\mathbf{h}(n)\right)$
   $\mathbf{P}(n) = \beta^{-1}\,\mathrm{Tri}\left\{\mathbf{P}(n-1) - \mathbf{g}(n)\,\mathbf{h}^{\mathrm{H}}(n)\right\}$
   $\mathbf{e}(n) = \mathbf{x}(n) - \hat{\mathbf{U}}_\mathbf{s}(n-1)\,\mathbf{y}(n)$
   $\hat{\mathbf{U}}_\mathbf{s}(n) = \hat{\mathbf{U}}_\mathbf{s}(n-1) + \mathbf{e}(n)\,\mathbf{g}^{\mathrm{H}}(n)$
   `end`

Table 6 – Summary of the PAST algorithm.

Where $\mathbf{x}(n)$ is the observed data vector at time instant (n). $\mathbf{P}(n)$ corresponds to the inverse of the correlation matrix of the projected vector $\mathbf{y}(n) = \hat{\mathbf{U}}_\mathbf{s}(n-1)\,\mathbf{x}(n)$. The vector $\mathbf{g}(n)$ is defined as the gain vector and $\mathbf{e}(n)$ is referred as the approximation error.

4.5 Proposed PAST-DoA/KRF

The proposed approach links the PAST algorithm to the DoA/KRF time-delay estimation technique by providing a signal subspace estimation at each time instant, instead of performing a full SVD on each observed epoch or on a K collection period of epochs. After obtaining an estimation for the signal subspace, the time delay estimation is performed according to the DoA/KRF technique previously discussed on Section (3.5).

Since PAST is based on RLS (Recursive Least Squares) [29] proposed a tensor-based version of PAST, which consists of processing the entire new batch of observations for a given n-mode unfolding $[\boldsymbol{\mathcal{Y}}]_{(n)}$. Recall that in this work the estimates are performed on the observed tensor's third-mode unfolding $[\boldsymbol{\mathcal{Y}}]_{(3)}$ therefore, the tensor-based PAST method will be implemented for the third-mode unfolding in order to provide a signal subspace estimation at each time instant (n). The pseudo-code of the proposed technique can be consulted in Table (7).

Notice that the tensor-based PAST technique consists of a rank-1 update of the estimated signal subspace matrix. The method does not provide the exact basis of eigenvectors related to the signal subspace of the covariance matrix of the observed data, but a mere basis to span it, which is sufficient for solving the shift invariance equation of ESPRIT and reconstruct the array steering factor matrix.

Algorithm 4 PAST-DoA/KRF Time-delay estimation

1. Initialization.
   $\mathbf{P}(0) = \mathbf{I}_R$
   $\hat{\mathbf{U}}_{\mathbf{s}}(0) = \mathbf{I}_{M \times R}$

2. Tensor-based PAST main section.

   `for` $n = 1, 2, \ldots$ `do:`
   $\mathbf{Y}(n) = \hat{\mathbf{U}}_{\mathbf{s}}^{\mathrm{H}}(n-1)\,[\boldsymbol{\mathcal{Y}}]_{(3)}(n)$
   $\mathbf{C}_{yy}(n) = \beta\,\mathbf{C}_{yy}(n-1) + \mathbf{Y}(n)\mathbf{Y}^{\mathrm{H}}(n)$
   $\mathbf{G}(n) = \mathbf{C}_{yy}^{-1}(n)\mathbf{Y}(n)$
   $\mathbf{E}(n) = [\boldsymbol{\mathcal{Y}}]_{(3)}(n) - \hat{\mathbf{U}}_{\mathbf{s}}(n-1)\,\mathbf{Y}(n)$
   $\hat{\mathbf{U}}_{\mathbf{s}}(n) = \hat{\mathbf{U}}_{\mathbf{s}}(n-1) + \mathbf{E}(n)\,\mathbf{G}^{\mathrm{H}}(n)$

   3. DoA/KRF main section: Table (5).
      3.1 Concerning the ESPRIT section, proceed direct to step (3) to solve the shift invariance equation by means of $\hat{\mathbf{U}}_{\mathbf{s}}(n)$ estimated previously.

   `end`

Table 7 – Summary of the proposed PAST-DoA/KRF algorithm.

4.6 Fast Data Projection Method - FDPM

The FDPM algorithm proposed by [26] is based on the power method derived from the numerical analysis [30]. For instance, given a non-zero matrix $\mathbf{W} \in \mathbb{C}^{M \times L}$ and a matrix $\mathbf{R} \in \mathbb{C}^{M \times M}$, the following simultaneous iteration:

Algorithm 5 Simultaneous iteration

`for` $n = 1, 2, \ldots$ `do:`
$$\mathbf{W}(i) = \frac{\mathbf{R}\mathbf{W}(i)}{||\mathbf{R}\mathbf{W}(i)||}$$
`end`

Table 8 – Power method for eigenvector tracking.

Converges to $\mathbf{W}(n)$ forming a basis for the greatest L eigenvectors of $\mathbf{R}$, i.e. they span the same subspace. However, depending on the scenario, at each successive iteration, orthogonalising $\mathbf{W}(i)$ and normalising its columns may be required. Thus, [31] proposed an iterative solution based on the adaptive orthogonal iteration algorithm. The resulting technique is referred as the Data Projection Method. Later, [26] introduced the Fast Data Projection Method (FDPM) algorithm which has complexity of $\mathcal{O}(NL)$ and provides stable subspace estimates with exponentially convergence towards orthonormality. The

method is detailed in the pseudo-algorithm presented in Table (9).

Algorithm 6 Fast Data Projection Method - FDPM [26]

1. Initialization.
   $\hat{\mathbf{U}}_{\mathbf{s}}(0) = \mathbf{I}_{M\times R}$
   $\mathbf{e}_1 = [1 \;\; 0_{M-1}]$
   Define the step size $\bar{\mu} = 1 - \beta$

2. FDPM main section.
   `for` $n = 1, 2, \ldots$ `do:`
   $\mathbf{r}(n) = \hat{\mathbf{U}}_{\mathbf{s}}(n-1)\,\mathbf{x}(n)$
   $\mathbf{T}(n) = \hat{\mathbf{U}}_{\mathbf{s}}(n-1) + \dfrac{\bar{\mu}}{||\mathbf{x}(n)||^2}\mathbf{x}(n)\mathbf{r}^{\mathrm{H}}(n)$
   $\mathbf{a}(n) = \mathbf{r}(n) - ||\mathbf{r}(n)||\,\mathbf{e}_1$
   $\mathbf{Z}(n) = \mathbf{T}(n)\dfrac{2}{||\mathbf{a}||^2}(\mathbf{T}(n)\,\mathbf{a}(n))\,\mathbf{a}^{\mathrm{H}}(n)$
   $\hat{\mathbf{U}}_{\mathbf{s}}(n) =$ normalize each column of$\{\mathbf{Z}(n)\}$
   `end`

Table 9 – Summary of the FDPM algorithm.

4.7 Proposed FDPM-DoA/KRF

The proposed approach links the FDPM algorithm to the DoA/KRF time-delay estimation technique by providing a signal subspace estimation at each time instant, instead of performing a full SVD on each observed epoch or on a K collection period of epochs. After obtaining an estimation for the signal subspace, the time delay estimation is performed according to the DoA/KRF technique previously discussed on Section (3.5).

As seen on Section (4.3) each upcoming epoch to be concatenated to the previous data provides a number of Q observation vectors. In this context, to update the signal subspace estimate $\hat{\mathbf{U}}_{\mathbf{s}}(n+1)$ the matrix-based FDPM method has to be modified in order to process a batch of Q columns. Therefore, as similarly as performed in [32] to a subspace tracking technique based on the power method, we propose the tensor-based version of the FDPM algorithm. It starts by considering each column of $\boldsymbol{\mathcal{Y}}_{(n+1)}$ as a new observation vector. The columns are processed sequentially, and in order to weight a batch of Q observation vectors, the forgetting factor is altered according to the index of each processed column. For instance, at a given time instant $(n+1)$ the first column of a batch of Q observation vectors from $\boldsymbol{\mathcal{Y}}_{(n+1)}$ is considered as the new observation vector, the forgetting factor stays the same as that used in the matrix-based case. For the second column, which is treated as the second equivalent observation vector, the forgetting factor is set to one. The proposed FDPM-DoA/KRF technique is detailed in the pseudo-algorithm shown in Table (9).

The purpose of adopting FDPM as a recursive update algorithm to $\hat{\mathbf{U}}_{\mathbf{s}}(n+1)$ is due to the output basis provided by the method, which is orthonormal, required if the array response does not satisfy the shift invariance equation. In this scenario, the array steering factor matrix can be rebuild by means of other subspace-based techniques that require this orthonormality, such as MUSIC [33].

Algorithm 7 FDPM-DoA/KRF Time-delay estimation

1. Initialization.
   $\hat{\mathbf{U}}_{\mathbf{s}}(0) = \mathbf{I}_{M\times R}$
   $\mathbf{e}_1 = [1 \;\; 0_{M-1}]$
   Define the step size $\bar{\mu} = 1 - \beta$

   `for` $n = 1, 2, \ldots$ `do:`

      2. Tensor-based FDPM main section.

      `for` $k = 1, 2, \ldots, Q$ `do:`
         `if` $k = 1$
            $\beta' = \beta$
         `else`
            $\beta' = 1$
         `end`

         $\mathbf{r}(k) = \hat{\mathbf{U}}_s(k-1)\,[\boldsymbol{\mathcal{Y}}_n]_{(3)_{(:,\,k)}}$
         $\mathbf{T}(k) = \hat{\mathbf{U}}_{\mathbf{s}}(k-1) + \dfrac{\bar{\mu}}{||[\boldsymbol{\mathcal{Y}}_n]_{(3)_{(:,\,k)}}||^2}[\boldsymbol{\mathcal{Y}}_n]_{(3)_{(:,\,k)}}\mathbf{r}^{\mathrm{H}}(k)$
         $\mathbf{a}(k) = \mathbf{r}(k) - ||\mathbf{r}(k)||\,\mathbf{e}_1$
         $\mathbf{Z}(k) = \mathbf{T}(k)\dfrac{2}{||\mathbf{a}||^2}(\mathbf{T}(k)\,\mathbf{a}(k))\,\mathbf{a}^{\mathrm{H}}(k)$
         $\hat{\mathbf{U}}_{\mathbf{s}}(k) =$ normalize each column of$\{\mathbf{Z}(k)\}$

      `end`

      3. DoA/KRF main section: Table (5).
      3.1 Concerning the ESPRIT section, proceed direct to step (3) to solve the shift invariance equation by means of $\hat{\mathbf{U}}_{\mathbf{s}}(n)$ estimated previously.

   `end`

Table 10 – Summary of the proposed FDPM-DoA/KRF algorithm.

4.8 Review on the computational complexity of the algorithms

In this assessment, the operation counts on the study of the computational complexity of the algorithms are expressed in terms of Multiply Accumulate (MAC) operations, referred as FLoating point OPeration (FLOP) counts [34] [35]. As similarly as considered in [15] some operations such as the unfolding and the inverse-unfolding are not taken into account in the computational complexity, since both functions are only about data representation rather than operating on the data. In addition, the stage of finishing the correlation by multiplying the solution vector by $\mathbf{\Sigma V}^H$ will also be ignored. Hence, this discussion is more about the relative complexity difference between each algorithm rather than their absolute complexity.

As the DoA/KRF scheme applies a SVD on a KQ collection of vectors of length M its complexity requires $\mathcal{O}(MKQ)$ operations. Considering the number of impinging signals as L, the computational complexity of FDPM-DoA/KRF requires $\mathcal{O}(ML\,Q)$ operations while the computational cost of PAST-DoA/KRF consists of $\mathcal{O}(ML)$ operations. Table (11) exposes the overall complexity of the algorithms.

Algorithm	**Complexity**
DoAKRF	$\mathcal{O}(MKQ)$
FDPMDoA/KRF	$\mathcal{O}(ML\,Q)$
PASTDoA/KRF	$\mathcal{O}(ML)$

Table 11 – Numerical complexity of the algorithms.

Notice in Table (11) that if the receiver decides to increase the number of collect epochs, the computational cost of DoA/KRF increases linearly while the complexity of the proposed techniques remains unaltered.

Part III

Simulations and results

5 Tracking Simulation

5.1 Simulation parameters

Similarly to [1] [15] we consider a scenario with a left centro-hermitian uniform linear array receiver with $M = 8$ elements and half-wavelength $\Delta = \lambda/2$ spacing. The GNSS signal is a GPS course acquisition PR code from D = 1 satellite at a carrier frequency $f_c = 1575.42$ MHz, bandwidth $B = 1.023$ MHz and chip duration $T_c = 1/B = 977.52$ ns with $N = 2046$ samples collected every k-th observation period during $K = 30$ epochs. Each epoch has duration $\Delta t = 1$ ms. The number of impinging signals on the receiver is $L = 2$, one LOS component with time-delay τ_{LOS} and one NLOS multipath replica with time-delay τ_{NLOS}, such that $\tau_{\text{NLOS}} = \tau_{\text{LOS}} + \Delta\tau$, where $\Delta\tau$ is the delay difference between each component. Their azimuth angle difference is $\Delta\phi = 25°$.

For the pre-processing techniques SPS/ESPS the array is divided into $L_s = 5$ subarrays with $M_s = 4$ elements each. Signal phases are independent and identically distributed $\sim$U$[0, 2\pi[$. The number of correlators in the bank is $Q = 11$ equally spaced between $-T_c$ and T_c. The carrier-to-noise ratio is $C/N0 = 48$ dB-Hz, resulting in a pre-correlation $\text{SNR}_{\text{pre}} = C/N_0 - 10\log_{10}(2B) \approx -15.11$ dB. Processing gain $G = 10\log_{10}(B\Delta t) \approx 30.1$ dB, post-correlation $\text{SNR}_{\text{post}} = \text{SNR}_{\text{pre}} + G \approx 15$ dB and signal to multipath ratio (SMR) of 5 dB.

For the tracking scenario, we consider a total of $N = 50$ received tensors. The length of the sliding window applied on the data is K= 30 epochs. The step variation of the angle of arrival between each acquired tensor is $\Delta\phi_n = 0.5°$. For the PAST subspace tracker, the forgetting factor $\beta_{\text{PAST}} = 0.95$. For the FDPM technique $\beta_{\text{FDPM}} = 0.97$.

The results are obtained by performing $M_c = 1000$ Monte Carlo (MC) simulations to plot the Root Mean Squared Error (RMSE) expressed in meters, which is a measurement of the estimated time-delay multiplied by the speed of light, $c = 299792458$ m/s. The expression is written as:

$$\text{RMSE}\,(\text{m}) = c\sqrt{\frac{1}{M_c}\sum_{i=1}^{M_c}(\tau_i - \hat{\tau}_i)^2} \tag{5.1}$$

The Orthonormality Subspace Root Mean Squared Error (OSRMSE) will measure how far the estimated subspaces are far from being orthornomal with respect to the identity matrix. The computation of the expression is given by:

$$\text{OSRMSE} = \sqrt{\frac{1}{M_c}\sum_{i=1}^{M_c}(||\mathbf{I} - (\hat{\mathbf{W}}_i\hat{\mathbf{W}}_i^{\text{H}})||_F^2)^2} \tag{5.2}$$

5.2 Simulation results

The RMSE (τ_{LOS}) [m] for the techniques: DoA/KRF, PAST-DoA/KRF and FDPM-DoA/KRF simulated in the tracking scenario with the parameters described before is presented in Figure (19).

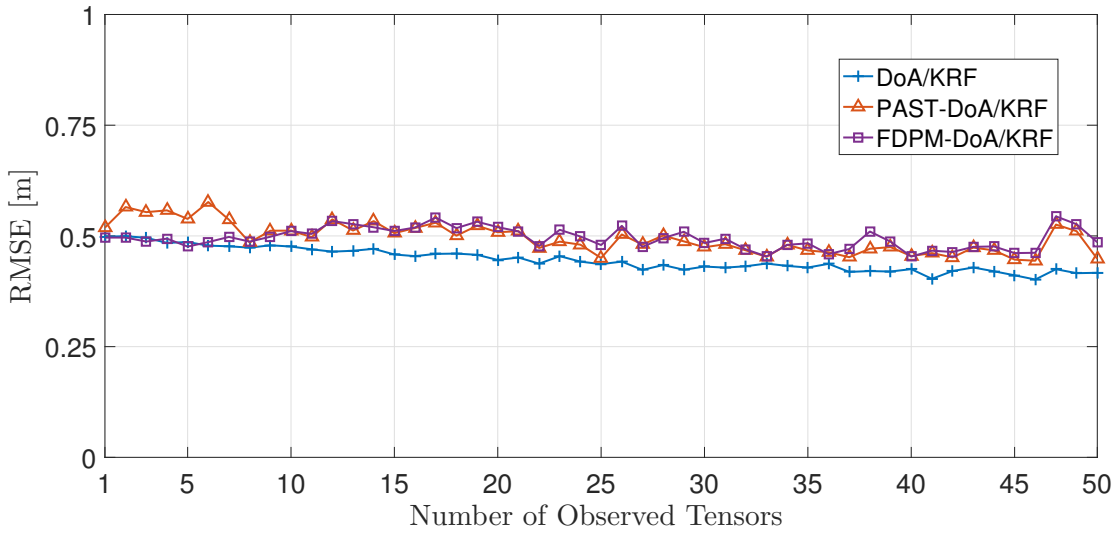

Figure 19 – RMSE in meters.

Notice that PAST-DoA/KRF and FDPM-DoA/KRF have similar performance. The average RMSE of both techniques is of 0.65 meters, which has a slight greater average when compared to DoA/KRF RMSE of 0.48 meters. In short we can affirm that the subspace-based tracking techniques achieve similar time-delay estimation performance with respect to DoA/KRF.

Concerning the Orthonormality Subspace RMSE of the proposed techniques, we observe in Figure (20) that the basis provided by FDPM-DoA/KRF is more close to orthornomality when compared to PAST-DoA/KRF.

On the computational cost of the simulation, we notice in Figure (21) that the results correspond to the theoretical computational complexity discussed in Section (4.8). In addition, PAST-DoA/KRF and FDPM-DoA/KRF have similar performance and show substantially lower complexity when compared to DoA/KRF.

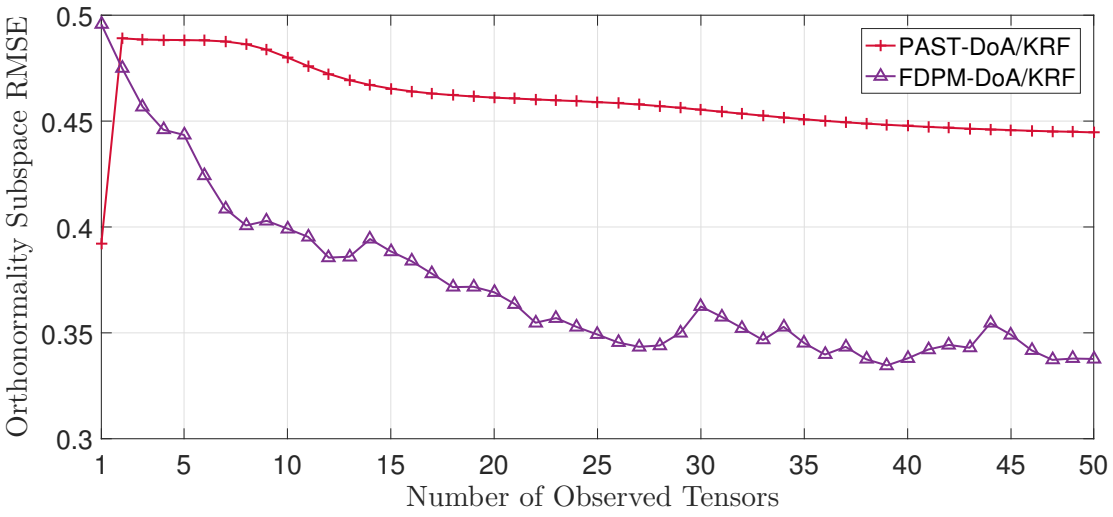

Figure 20 – Orthonormality Subspace RMSE for the subspace-based tracking techniques.

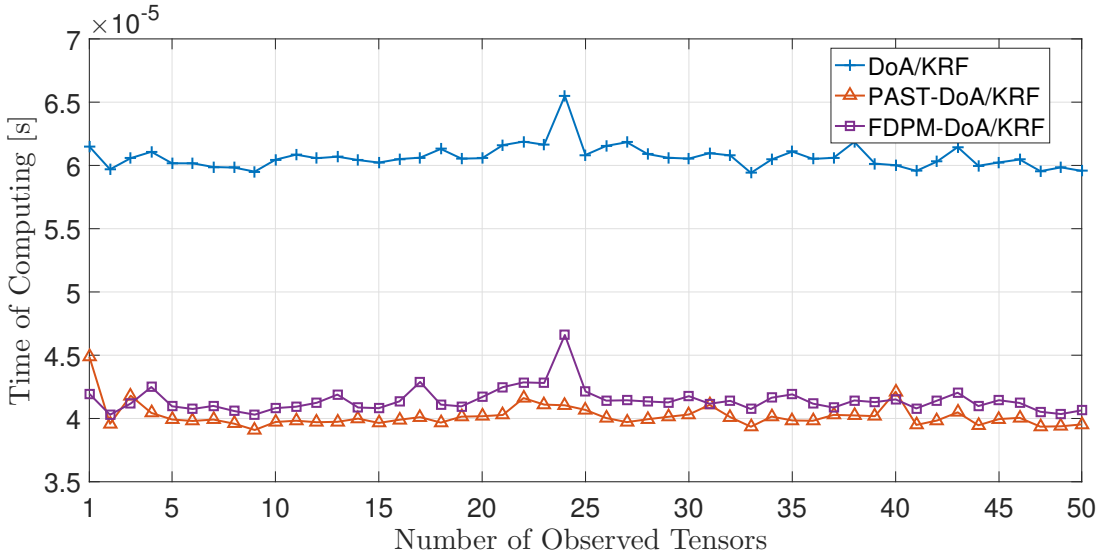

Figure 21 – Time of Computing (ToC) of the simulation.

5.3 Conclusion

In this work we proposed two subspace-based tracking techniques that achieve similar time-delay estimation performance with respect to the studied state-of-the-art technique. Concerning the computational complexity, both proposed approaches provide a lower computational cost.

Bibliography

1 LIMA, D. V. d. et al. High Resolution Time-Delay Estimation via Direction of Arrival Estimation and Khatri-Rao Factorization for Multipath Mitigation. In: *WSA 2017; 21th International ITG Workshop on Smart Antennas*. [S.l.: s.n.], 2017. p. 1–8.

2 KOLDA, T. G.; BADER, B. W. Tensor Decompositions and Applications. *SIAM REVIEW*, v. 51, n. 3, p. 455–500, 2009.

3 ROEMER, F. *Advanced Algebraic Concepts for Efficient Multi-Channel Signal Processing*. [S.l.].

4 SOUBIELLE, J. et al. GPS positioning in a multipath environment. *IEEE Transactions on Signal Processing*, v. 50, n. 1, p. 141–150, 2002.

5 NEE, R. van et al. The multipath estimating delay lock loop: approaching theoretical accuracy limits. In: *Proceedings of 1994 IEEE Position, Location and Navigation Symposium - PLANS'94*. [S.l.]: IEEE. p. 246–251. ISBN 0-7803-1435-2.

6 TEUNISSEN, P. J.; MONTENBRUCK, O. (Ed.). *Springer Handbook of Global Navigation Satellite Systems*. Cham: Springer International Publishing, 2017. ISBN 978-3-319-42926-7.

7 ANTONINI, M. et al. Vehicular remote tolling services using EGNOS. In: *PLANS 2004. Position Location and Navigation Symposium (IEEE Cat. No.04CH37556)*. [S.l.: s.n.], 2004. p. 375–379.

8 KANG, C.; LEE, S.; CHUNG, C. C. On-Road Vehicle Localization with GPS under Long Term Failure of a Vision Sensor. In: *2015 IEEE 18th International Conference on Intelligent Transportation Systems*. [S.l.: s.n.], 2015. p. 1638–1643. ISSN 2153-0017.

9 UCHIDA, K. et al. Development of automatic system for monitoring fishing effort in conger-eel tube fishery using radio frequency identification and global positioning system. *Fisheries Science*, John Wiley & Sons, Ltd (10.1111), v. 71, n. 5, p. 992–1002, 10 2005.

10 ESAU, T. et al. Economic analysis for smart sprayer application in wild blueberry fields. *Precision Agriculture*, Springer US, v. 17, n. 6, p. 753–765, 12 2016.

11 DUNN, M. *INTERFACE SPECIFICATION IS-GPS-200. NAVSTAR GPS Space Segment/Navigation User Segment Interface*. [S.l.], 2018.

12 BORRE, K. K. *A software-defined GPS and Galileo receiver : a single-frequency approach*. [S.l.]: Birkhauser, 2007. 176 p. ISBN 9780817643904.

13 CHEN, Z.; GOKEDA, G.; YU, Y. *Introduction to direction-of-arrival estimation*. [S.l.]: Artech House, 2010. 193 p. ISBN 1596930896.

14 ROY, R.; KAILATH, T. ESPRIT-estimation of signal parameters via rotational invariance techniques. *IEEE Transactions on Acoustics, Speech, and Signal Processing*, v. 37, n. 7, p. 984–995, 1989. ISSN 0096-3518.

15 HAMMOUD, B. et al. Tensor-Based Approach for Time-Delay Estimation. In: *WSA 2016; 20th International ITG Workshop on Smart Antennas*. [S.l.: s.n.], 2016. p. 1–7.

16 SELVA, J. *Efficient Multipath Mitigation in Navigation Systems*. [S.l.], 2004.

17 LIMA, D. V. de et al. Time-Delay estimation via CPD-GEVD applied to tensor-based GNSS arrays with errors. In: *2017 IEEE 7th International Workshop on Computational Advances in Multi-Sensor Adaptive Processing (CAMSAP)*. [S.l.]: IEEE, 2017. p. 1–5. ISBN 978-1-5386-1251-4.

18 ZANATTA, M. d. R. Tensor-based time-delay estimation techniques for third generation global positioning system. 2 2018.

19 ROEMER, F.; HAARDT, M. Tensor-based channel estimation (TENCE) for two-way relaying with multiple antennas and spatial reuse. In: *2009 IEEE International Conference on Acoustics, Speech and Signal Processing*. [S.l.]: IEEE, 2009. p. 3641–3644. ISBN 978-1-4244-2353-8.

20 PILLAI, S.; KWON, B. Forward/backward spatial smoothing techniques for coherent signal identification. *IEEE Transactions on Acoustics, Speech, and Signal Processing*, v. 37, n. 1, p. 8–15, 1 1989.

21 Tie-Jun Shan; WAX, M.; KAILATH, T. On spatial smoothing for direction-of-arrival estimation of coherent signals. *IEEE Transactions on Acoustics, Speech, and Signal Processing*, v. 33, n. 4, p. 806–811, 8 1985.

22 GOMES, P. R. et al. Tensor-based methods for blind spatial signature estimation under arbitrary and unknown source covariance structure. *Digital Signal Processing*, Academic Press, v. 62, p. 197–210, 3 2017.

23 NION, D.; SIDIROPOULOS, N. D. Adaptive Algorithms to Track the PARAFAC Decomposition of a Third-Order Tensor. *IEEE Transactions on Signal Processing*, v. 57, n. 6, p. 2299–2310, 2009. ISSN 1053-587X.

24 BADEAU, R.; RICHARD, G.; DAVID, B. Fast and Stable YAST Algorithm for Principal and Minor Subspace Tracking. *IEEE Transactions on Signal Processing*, v. 56, n. 8, p. 3437–3446, 2008. ISSN 1053-587X.

25 ADALI, T.; HAYKIN, S. S. *Adaptive signal processing : next generation solutions*. [S.l.]: IEEE, Institute of Electrical and Electronics Engineers, 2010. 407 p. ISBN 0470195177.

26 DOUKOPOULOS, X. G.; MOUSTAKIDES, G. V. The fast Data Projection Method for stable subspace tracking. In: *2005 13th European Signal Processing Conference*. [S.l.: s.n.], 2005. p. 1–4.

27 YANG, B. Projection approximation subspace tracking. *IEEE Transactions on Signal Processing*, v. 43, n. 1, p. 95–107, 1 1995. ISSN 1053-587X.

28 DOUKOPOULOS, X. G.; MOUSTAKIDES, G. V. Fast and Stable Subspace Tracking. *IEEE Transactions on Signal Processing*, v. 56, n. 4, p. 1452–1465, 2008. ISSN 1053-587X.

29 ROEMER, F. et al. Tensor subspace tracking via Kronecker structured projections (TeTraKron). In: *2013 5th IEEE International Workshop on Computational Advances in Multi-Sensor Adaptive Processing (CAMSAP)*. [S.l.]: IEEE, 2013. p. 212–215. ISBN 978-1-4673-3146-3.

30 GOLUB, G. H. G. H.; LOAN, C. F. V. *Matrix computations*. [S.l.]: Johns Hopkins University Press, 1996. 694 p. ISBN 0801854148.

31 YANG, J.-F.; KAVEH, M. Adaptive eigensubspace algorithms for direction or frequency estimation and tracking. *IEEE Transactions on Acoustics, Speech, and Signal Processing*, v. 36, n. 2, p. 241–251, 1988.

32 CHENG, Y. et al. Tensor subspace Tracking via Kronecker structured projections (TeTraKron) for time-varying multidimensional harmonic retrieval. *EURASIP Journal on Advances in Signal Processing*, Springer International Publishing, v. 2014, n. 1, p. 123, 12 2014.

33 SCHMIDT, R. O. *A signal subspace approach to multiple emitter location and spectral estimation /*. [S.l.: s.n.], 1981.

34 STOTHERS, A. J. On the Complexity of Matrix Multiplication. 2010.

35 HALKO, N.; MARTINSSON, P.; TROPP, J. Finding Structure with Randomness: Probabilistic Algorithms for Constructing Approximate Matrix Decompositions. *SIAM Review*, v. 53, n. 2, p. 217–288, 2011.

36 LATHAUWER, L. D.; MOOR, B. D.; VANDEWALLE, J. On the Best Rank-1 and Rank-R Approximation of Higher-Order Tensors. *SIAM Journal on Matrix Analysis and Applications*, Society for Industrial and Applied Mathematics, v. 21, n. 4, p. 1324–1342, 1 2000.

37 HARSHMAN, R. A. *PARAFAC2: Mathematical and technical notes*. Michigan, 1972. 30–44 p.

38 KRUSKAL, J. B. Three-way arrays: rank and uniqueness of trilinear decompositions, with application to arithmetic complexity and statistics. *Linear Algebra and its Applications*, North-Holland, v. 18, n. 2, p. 95–138, 1 1977.

Appendix

APPENDIX A – Matrix operations

In this section, matrix operations employed in the conception of the data model derived in Chapter (3) are presented.

A.1 The Kronecker product

The Kronecker product of two matrices $\mathbf{A} \in \mathbb{C}^{I\times J}$ and $\mathbf{B} \in \mathbb{C}^{K\times L}$ is a matrix of dimensions $IK \times JL$. The product is defined as:

$$\mathbf{A} \otimes \mathbf{B} = \begin{bmatrix} a_{1,1}\mathbf{B} & a_{1,2}\mathbf{B} & \cdots & a_{1,J}\mathbf{B} \\ a_{2,1}\mathbf{B} & a_{2,2}\mathbf{B} & \cdots & a_{2,J}\mathbf{B} \\ \vdots & \vdots & \vdots & \vdots \\ a_{I,1}\mathbf{B} & a_{I,2}\mathbf{B} & \ddots & a_{I,J}\mathbf{B} \end{bmatrix} \in \mathbb{C}^{IJ\times KL} \tag{A.1}$$

A.2 The Khatri-Rao product

The Khatri-Rao product of two matrices $\mathbf{A} \in \mathbb{C}^{I\times J}$ and $\mathbf{B} \in \mathbb{C}^{K\times L}$ is a matrix of dimensions $IK \times L$. The product is defined as:

$$\mathbf{A} \diamond \mathbf{B} = \begin{bmatrix} a_{1,1}\mathbf{b}_1 & a_{1,2}\mathbf{b}_2 & \cdots & a_{1,J}\mathbf{b}_L \\ a_{2,1}\mathbf{b}_1 & a_{2,2}\mathbf{b}_2 & \cdots & a_{1,J}\mathbf{b}_L \\ \vdots & \vdots & \vdots & \vdots \\ a_{I,1}\mathbf{b}_1 & a_{I,2}\mathbf{b}_2 & \cdots & a_{I,J}\mathbf{b}_L \end{bmatrix} \tag{A.2}$$

$$= \begin{bmatrix} \mathbf{a}_1 \otimes \mathbf{b}_1 & \mathbf{a}_2 \otimes \mathbf{b}_2 & \cdots & \mathbf{a}_L \otimes \mathbf{b}_L \end{bmatrix} \in \mathbb{C}^{IK\times L} \tag{A.3}$$

A.3 Outer product

The outer product of two vectors $\mathbf{a} \in \mathbb{C}^{I\times 1}$ and $\mathbf{b} \in \mathbb{C}^{J\times 1}$ results in a matrix of dimensions $I \times J$. The product is defined as:

$$\mathbf{a} \circ \mathbf{b} = \mathbf{a}\mathbf{b}^{\mathrm{T}} = \begin{bmatrix} a_1 b_1 & a_1 b_2 & \cdots & a_1 b_J \\ a_2 b_1 & a_2 b_2 & \cdots & a_2 b_J \\ \vdots & \vdots & \ddots & \vdots \\ a_I b_1 & a_I b_2 & \cdots & a_I b_J \end{bmatrix} \in \mathbb{C}^{I\times J} \tag{A.4}$$

Notice that the outer product of three vectors results in a tensor, such that:

$$\boldsymbol{\mathcal{D}} = \mathbf{a} \circ \mathbf{b} \circ \mathbf{c} \in \mathbb{C}^{I\times J\times K} \tag{A.5}$$

Where $\mathbf{c} \in \mathbb{C}^{K\times 1}$.

A.4 The vec{ } operator

Denoting $\mathbf{a}_i$ as the i-th column of a matrix $\mathbf{A} \in \mathbb{C}^{I\times J}$. The vec operator stacks the columns of $\mathbf{A}$ in a single vector resulting:

$$\text{vec}\{\mathbf{A}\} = \begin{bmatrix} \mathbf{a}_1 \\ \vdots \\ \mathbf{a}_J \end{bmatrix} \in \mathbb{C}^{IJ\times 1} \tag{A.6}$$

Another important propriety of the vec operator is for $\mathbf{X} = \mathbf{ABC}$, where $\mathbf{A} \in \mathbb{C}^{I\times J}$, $\mathbf{B} \in \mathbb{C}^{I\times I}$ is a diagonal matrix and $\mathbf{C} \in \mathbb{C}^{I\times K}$.

$$\text{vec}\{\mathbf{ABC}\} = \left(\mathbf{C}^{\text{T}} \diamond \mathbf{A}\right) \text{diag}\{\mathbf{B}\} \in \mathbb{C}^{IK} \tag{A.7}$$

A.5 The unvec{ } operator

The unvec operator concatenates a chosen amount of columns of a vector $\mathbf{a} = \left[\mathbf{a}_1, \cdots, \mathbf{a}_J\right] \in \mathbb{C}^{IJ\times 1}$ forming a matrix $\mathbf{A} \in \mathbb{C}^{I\times J}$. Where $\mathbf{a}_i \in \mathbb{C}^{1\times J}$ denotes a group of J elements in the vector $\mathbf{a}$.

The result of the unvec operator is given by:

$$\text{unvec}\{\mathbf{a}\} = \begin{bmatrix} \mathbf{a}_1 & \mathbf{a}_2 & \cdots & \mathbf{a}_3 \end{bmatrix} \in \mathbb{C}^{I\times K} \tag{A.8}$$

A.6 The Singular Value Decomposition

Every matrix $\mathbf{M}$ that has it's entries from the real or the complex domain, admits a factorization called Singular Value Decomposition (SVD) in such a way that for $\mathbf{M} \in \mathbb{C}^{M\times N}$:

$$\mathbf{M} = \mathbf{U}\mathbf{\Sigma}\mathbf{V}^{\text{H}} \tag{A.9}$$

Where $\mathbf{U} \in \mathbb{C}^{M\times M}$ is an unitary matrix, $\mathbf{\Sigma} \in \mathbb{C}N \times N$ is a diagonal matrix and $\mathbf{V} \in \mathbb{C}^{N\times N}$ is an unitary matrix.

A.7 The Khatri-Rao factorization

Given the Khatri-Rao product: $(\mathbf{A} \diamond \mathbf{B}) = \begin{bmatrix} \mathbf{a}_1 \otimes \mathbf{b}_1 & \cdots & \mathbf{a}_{\text{R}} \otimes \mathbf{b}_{\text{R}} \end{bmatrix} \in \mathbb{C}^{IJ\times R}$ between the matrices $\mathbf{A} \in \mathbb{C}^{I\times R}$ $\mathbf{B} \in \mathbb{C}^{J\times R}$ each element $\mathbf{a}_{\text{r}} \otimes \mathbf{b}_{\text{r}}$ can be reshaped in such a way that:

$$\underset{J\times I}{\text{unvec}}\{\mathbf{a}_{\text{r}} \otimes \mathbf{b}_{\text{r}}\} = \begin{bmatrix} a_{1,\text{r}}b_{1,\text{r}} & \cdots & a_{\text{I},\text{r}}b_{1,\text{r}} \\ \vdots & \vdots & \vdots \\ a_{1,\text{r}}b_{J,\text{r}} & \cdots & a_{\text{I},\text{r}}b_{\text{J},\text{r}} \end{bmatrix} \in \mathbb{C}^{J\times I} \tag{A.10}$$

The structure of the matrix obtained in Equation (A.10) is equivalent to the following operation:

$$\underset{J\times I}{\text{unvec}}\{\mathbf{a}_\text{r} \otimes \mathbf{b}_\text{r}\} = \mathbf{b_r}\, \mathbf{a}_\text{r}^\text{T} \tag{A.11}$$

Where each $\mathbf{a}_\text{r}$ and $\mathbf{b}_\text{r}$ can be estimated using a rank-1 singular value decomposition:

$$\mathbf{b}_\text{r}\mathbf{a}_\text{r}^\text{T} = \mathbf{u}_\text{r}\, s_\text{r}\, \left(\mathbf{v}_\text{r}{}^*\right)^\text{T} \tag{A.12}$$

The estimations are then obtained by taking the square root of the singular value to distribute to the singular vector, such that:

$$\hat{\mathbf{a}}_\text{r} = \mathbf{v}_\text{r}{}^*\sqrt{s_\text{r}} \tag{A.13}$$

$$\hat{\mathbf{b}}_\text{r} = \mathbf{u}_\text{r}\sqrt{s_\text{r}} \tag{A.14}$$

APPENDIX B – Adaptive Array Signal Processing Techniques

B.1 Estimation of the Array Covariance Matrix

The nature of the GPS received signal is not deterministic, which means that for performing signal processing operations it is necessary to resort to the stochastic theory. Due to the need to perform autocorrelation operations, the received signal covariance matrix is defined as:

$$\mathbf{R}_{xx} = \mathrm{E}\{\mathbf{X}\mathbf{X}^{\mathrm{H}}\} \tag{B.1}$$

Taking into account the N amount of signal samples, the stochastic theory provides an approximation for the signal covariance matrix such that:

$$\hat{\mathbf{R}}_{xx} = \frac{1}{N}\sum_{n=1}^{N}\mathbf{x}[n]\mathbf{x}^{\mathrm{H}}[n] = \frac{1}{N}\mathbf{X}\mathbf{X}^{\mathrm{H}} \tag{B.2}$$

Where: $\lim_{N\to\infty}\hat{\mathbf{R}}_{xx} = \mathbf{R}_{xx}$

B.2 Forward Backward Averaging

The Forward Backward Averaging technique is capable of decorrelating signals and allowing the improving and application of subspace based methods for DoA estimation. For an uniform linear array (ULA) let the matrices $\mathbf{\Pi}_M \in \mathbb{Z}^{M\times M}$ e $\mathbf{\Pi}_N \in \mathbb{Z}^{N\times N}$, definided below:

$$\mathbf{\Pi}_M = \begin{bmatrix} 0 & 0 & 0 & & 1 \\ 0 & 0 & \vdots & & 0 \\ 0 & \vdots & 1 & \vdots & 0 \\ \vdots & 1 & 0 & & 0 \\ 1 & 0 & 0 & & 1 \end{bmatrix} \in \mathbb{Z}^{M\times M} \qquad \mathbf{\Pi}_N = \begin{bmatrix} 0 & 0 & 0 & & 1 \\ 0 & 0 & \vdots & & 0 \\ 0 & \vdots & 1 & \vdots & 0 \\ \vdots & 1 & 0 & & 0 \\ 1 & 0 & 0 & & 1 \end{bmatrix} \in \mathbb{Z}^{N\times N} \tag{B.3}$$

The ULA is considered a centro-hermitian antenna array due to the following propriety being satisfied:

$$\mathbf{R}_{xx} = \mathbf{\Pi}_M\mathbf{R}_{xx}\mathbf{\Pi}_N \tag{B.4}$$

The presented technique enables doubling the number of samples for the array configuration. Dimensional size reduction will not occur. The technique is used according to Equation:

$$\mathbf{X_{FBA}} = [\mathbf{X}|\mathbf{\Pi_M}\mathbf{X}^*\mathbf{\Pi_N}] \in \mathbb{C}^{M\times 2N} \tag{B.5}$$

B.3 Spatial Smoothing

In scenarios where more than two highly correlated sources are present the FBA cannot by itself restore the full rank of the signal covariance matrix. Therefore Spatial Smoothing presents as another solution. This technique divides the ULA into multiple subarrays as shown in Figure (22).

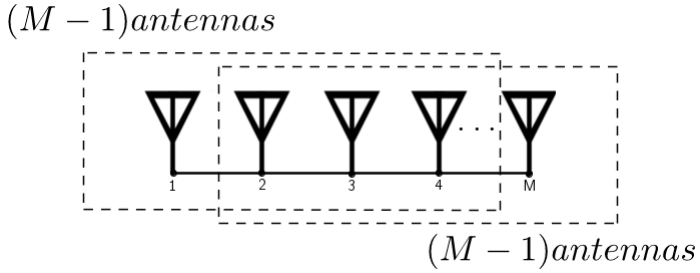

Figure 22 – Example of subarrays.

The steering vector for subarray 1 considering the ℓ-th impinging wave is given by:

$$\mathbf{a}_1(\theta_\ell) = \begin{bmatrix} 1 & e^{j\omega\tau_\ell} & (\cdots) & e^{(M-2)j\omega\tau_\ell} \end{bmatrix}^{\mathrm{T}} \in \mathbb{C}^{(M-1)\times L} \tag{B.6}$$

The steering matrix is obtained by concatenating the steering vectors for each signal received by the array:

$$\mathbf{A}_1(\theta_\ell) = \begin{bmatrix} \mathbf{a}_1(\theta_1) & \mathbf{a}_1(\theta_2) & (\cdots) & \mathbf{a}_1(\theta_L) \end{bmatrix} \in \mathbb{C}^{(M-1)\times L} \tag{B.7}$$

The steering vector for subarray 2 considering the l-th impiging wave is given by:

$$\mathbf{a}_2(\theta_\ell) = \begin{bmatrix} e^{j\omega\tau_\ell} & e^{2j\omega\tau_\ell} & (\cdots) & e^{(M-1)j\omega\tau_\ell} \end{bmatrix}^{\mathrm{T}} \in \mathbb{C}^{(M-1)\times L} \tag{B.8}$$

The steerig matrix is obtained by concatenating the stering vectors for each signal recceived by the array:

$$\mathbf{A}_2(\theta_\ell) = \begin{bmatrix} \mathbf{a}_2(\theta_1) & \mathbf{a}_2(\theta_2) & (\cdots) & \mathbf{a}_2(\theta_L) \end{bmatrix} \in \mathbb{C}^{(M-1)\times L} \tag{B.9}$$

The received signal model for each one of the subarrays can be described as:

$$\mathbf{X}_1 = \mathbf{A}_1\mathbf{S} + \mathbf{N}_1 \quad \in \mathbb{C}^{M-1\times L} \tag{B.10}$$

$$\mathbf{X}_2 = \mathbf{A}_2\mathbf{S} + \mathbf{N}_2 \quad \in \mathbb{C}^{M-1\times L} \tag{B.11}$$

The dimension of the matrices $\mathbf{A}_1$ and $\mathbf{A}_2$ is reduced leading to a reduced steering matrix of each subarray. However, it is possible to express the received signal without any loss of structure by concatenating these matrices.

Let the matrix $\mathbf{\Omega} \in \mathbb{C}^{L \times L}$ given by:

$$\mathbf{\Omega} = \begin{bmatrix} e^{j\omega\tau_1} & e^{j\omega\tau_2} & \dots & e^{j\omega\tau_L} \\ e^{j\omega\tau_1} & e^{j\omega\tau_2} & \dots & e^{j\omega\tau_L} \\ \vdots & \vdots & \vdots & \vdots \\ e^{j\omega\tau_1} & e^{j\omega\tau_2} & \dots & e^{j\omega\tau_L} \end{bmatrix} \in \mathbb{C}^{L \times L} \tag{B.12}$$

Considering the following relation:

$$\mathbf{A}_2 = \mathbf{A}_1 o\, \mathbf{\Omega} \tag{B.13}$$

Where o denotes the Hadamard product.

The matrix obtained throught the SPS techinique $\mathbf{X_{SPS}}$ has the double ammount of samples when compared to the original received signal matrix such that:

$$\mathbf{X_{SPS}} = \Big[\mathbf{X}_1 | \mathbf{X}_2\Big] = \Big[\mathbf{A}_1\mathbf{S} | \mathbf{A}_1 o\, \mathbf{\Omega}\Big] + \Big[\mathbf{N}_1 | \mathbf{N}_2\Big] \in \mathbb{C}^{M-1 \times 2N} \tag{B.14}$$

It is important to mention that it is possible to apply FBA on the covariance matrice of each subarray.

APPENDIX C – Tensor Calculus Concepts

In this section, general tensor-based operations necessary for deriving the techniques presented in the Chapters (3) and (4) are presented.

C.1 Tensors

In the same way vectors can be seen as a set of scalars, and matrices as a set of vectors, tensors can be viewed as a set of matrices, however, while matrices are limited to only two dimensions, tensors can have an unlimited number of dimensions. In this context, an N-dimensional tensor is denoted as $\boldsymbol{\mathcal{X}} \in \mathbb{C}^{M_1 \times M_2 \cdots \times M_n \cdots \times M_R}$. In addition, tensors can be seen as a collection of n-mode vectors, which are obtained if a given n-th index is varied and all other indices are kept fixed. For instance, given a third-order tensor $\boldsymbol{\mathcal{X}} \in \mathbb{C}^{I \times J \times K}$, its n-mode vectors are given by: $\{\mathbf{x}_{(i,:,:)} \ \ \mathbf{x}_{(:,j,:)} \ \ \mathbf{x}_{(:,:,k)}\}$. Figure (23) illustrates the n-modes vectors of a third order tensor.

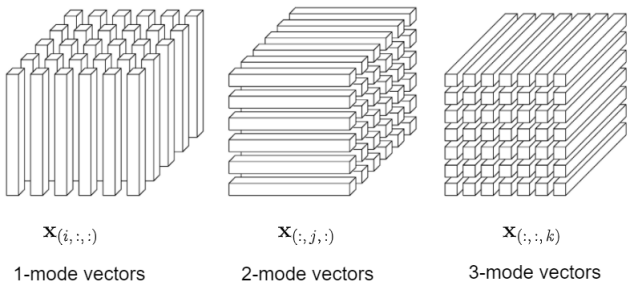

Figure 23 – N-modes vectors of a third order tensor. Figure adapted from [2].

C.2 The n-mode unfolding

The n-mode unfolding is a process that reorders the elements of a N-order tensor into a matrix. This is done by rearranging the n-modes vectors of the tensor to be the columns of the resulting matrix. Different works sometimes use different orderings. The notation adopted in this work is consistent to [3].

The column ordering chosen in this work is referred as the reverse cyclical unfolding, proposed in [36] which starts with the $(n-1)$-th index and proceeds backwards, up to the $(n+1)$-th index. Figure (24) illustrates this process for a third-order tensor of dimensions 4 x 5 x 3.

Proprieties of the n-mode unfoldings are discussed in Sections (C.4) and (C.3).

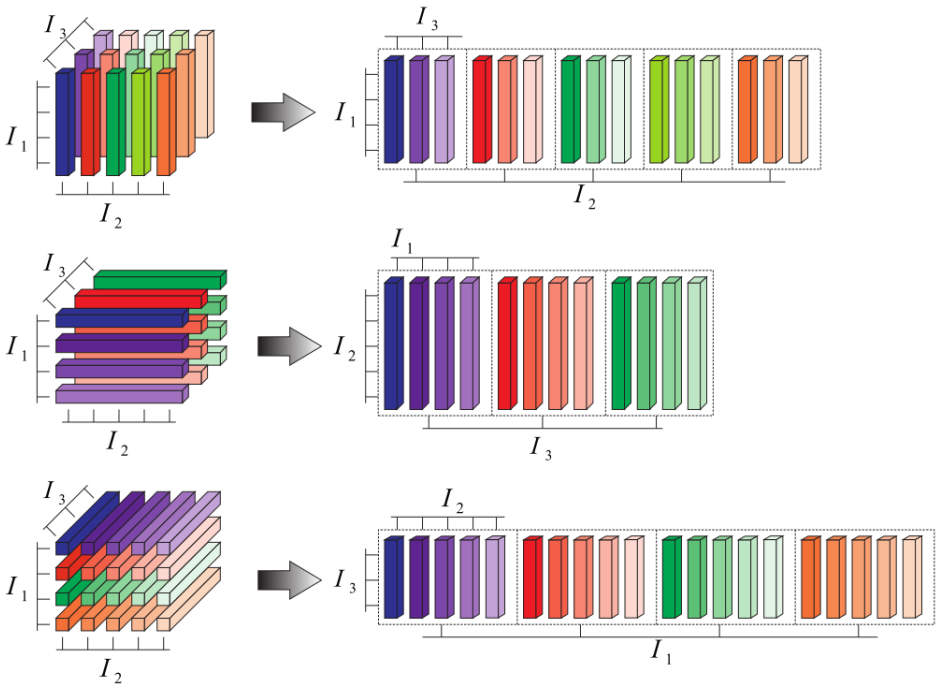

Figure 24 – Unfoldings in reverse cyclical column ordering of a third-order tensor of dimensions 4 x 5 x 3. Figure adapted from [3].

C.3 The n-mode product

A tensor can be multiplied by a matrix by means of the n-mode product. For an N-order tensor $\boldsymbol{\mathcal{X}} \in \mathbb{C}^{M_1 \times M_2 \cdots \times M_n \cdots \times M_R}$ and a matrix $\mathbf{B} \in \mathbb{C}^{M \times M_n}$, the n-mode product of these two terms is given by:

$$\boldsymbol{\mathcal{X}} \times_n \mathbf{B} = \mathbf{B}\,[\boldsymbol{\mathcal{X}}]_{(n)} \tag{C.1}$$

Where $[\boldsymbol{\mathcal{X}}]_{(n)} \in \mathbb{C}^{M_n \times M_1 M_2 \ldots M_N}$ is the n-mode unfolding of $\boldsymbol{\mathcal{X}}$. The output tensor is the matrix product of Equation (C.1) folded back into a tensor of size $M_1 \times M_2 \cdots \times M \cdots \times M_R$.

C.4 The PARAFAC decomposition

The Parallel Factor Analysis (PARAFAC) [37] is a polyadic form of a tensor. It expresses a given tensor as the sum of a finite number of rank-one tensors. For instance, given a R-rank third-order tensor $\boldsymbol{\mathcal{X}} \in \mathbb{C}^{I \times J \times K}$ the following expression:

$$\boldsymbol{\mathcal{X}} \approx \sum_{r=1}^{R} \mathbf{a} \circ \mathbf{b} \circ \mathbf{c} \in \mathbb{C}^{I \times J \times K} \tag{C.2}$$

Factorizes the tensor $\boldsymbol{\mathcal{X}}$ into a sum of component rank-one tensors. The factor matrices are referred as the combination of the vectors from each one of the rank-one

components. Therefore, the factor matrices associated to the PARAFAC decomposition of the tensor $\boldsymbol{\mathcal{X}}$ are written as:

$$\mathbf{A} = \begin{bmatrix} \mathbf{a}_1 & \cdots & \mathbf{a}_R \end{bmatrix} \in \mathbb{C}^{I \times R} \tag{C.3}$$

$$\mathbf{B} = \begin{bmatrix} \mathbf{b}_1 & \cdots & \mathbf{b}_R \end{bmatrix} \in \mathbb{C}^{J \times R} \tag{C.4}$$

$$\mathbf{C} = \begin{bmatrix} \mathbf{c}_1 & \cdots & \mathbf{c}_R \end{bmatrix} \in \mathbb{C}^{K \times R} \tag{C.5}$$

Under the condition of uniqueness [23] (when criteria involving the rank of the studied tensor and the size its factors matrices are satisfied [38]) the PARAFAC decomposition of a tensor can be expressed in terms of its factor matrices, such that:

$$\boldsymbol{\mathcal{X}} = \boldsymbol{\mathcal{I}}_{3,R} \times_1 \mathbf{A} \times_2 \mathbf{B} \times_3 \mathbf{C} \in \mathbb{C}^{I \times J \times K} \tag{C.6}$$

A propriety is that for a given third-order tensor that follows Equation (C.6) its unfoldings can be expressed by:

$$[\boldsymbol{\mathcal{X}}]_{(1)} = \mathbf{A} \left(\mathbf{B} \diamond \mathbf{C}\right)^{\mathrm{T}} \in \mathbb{C}^{I \times JK} \tag{C.7}$$

$$[\boldsymbol{\mathcal{X}}]_{(2)} = \mathbf{B} \left(\mathbf{C} \diamond \mathbf{A}\right)^{\mathrm{T}} \in \mathbb{C}^{J \times KI} \tag{C.8}$$

$$[\boldsymbol{\mathcal{X}}]_{(3)} = \mathbf{C} \left(\mathbf{A} \diamond \mathbf{B}\right)^{\mathrm{T}} \in \mathbb{C}^{K \times IJ} \tag{C.9}$$